Structure

Nanobodies targeting LexA autocleavage disclose a novel suppression strategy of SOS-response pathway

Graphical abstract

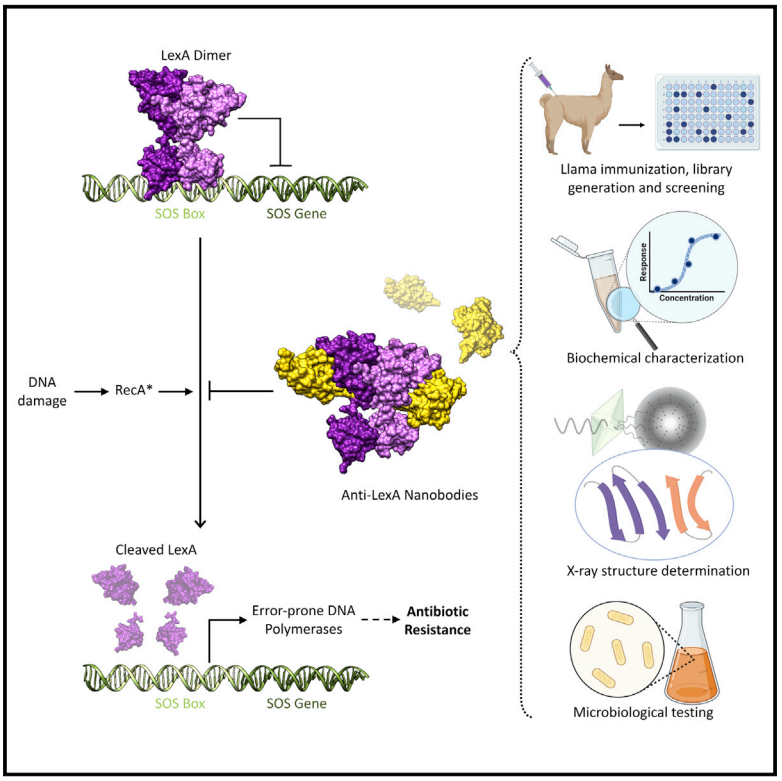

Highlights

- Nanobodies (NbSOSs) binding *Escherichia coli* LexA with nanomolar affinity have been discovered
- NbSOSs can inhibit LexA autoproteolysis and block the SOS response axis in bacteria
- Biophysical characterization of NbSOSs-LexA complexes discloses inhibition mechanism

Authors

Lorenzo Maso, Filippo Vascon, Monica Chinellato, ..., Jan Steyaert, Donatella Tondi, Laura Cendron

Correspondence

laura.cendron@unipd.it

In brief

Maso and colleagues discovered llama-derived nanobodies targeting transcriptional repressor LexA from *Escherichia coli*. The authors demonstrated that such binders can inhibit RecA stimulated autoproteolysis of LexA, thus blocking the SOS response activation, which is one of the most conserved mechanisms that fuel antimicrobial resistance acquisition in bacterial pathogens.

Maso et al., 2022, Structure *30*, 1479–1493
November 3, 2022
https://doi.org/10.1016/j.str.2022.09.004

Structure

CellPress

Article

Nanobodies targeting LexA autocleavage disclose a novel suppression strategy of SOS-response pathway

Lorenzo Maso,[1,9] Filippo Vascon,[1,9] Monica Chinellato,[1] Frédéric Goormaghtigh,[2,3] Pierangelo Bellio,[4] Enrica Campagnaro,[1] Laurence Van Melderen,[3] Maria Ruzzene,[5] Els Pardon,[6] Alessandro Angelini,[7] Giuseppe Celenza,[4] Jan Steyaert,[6] Donatella Tondi,[8] and Laura Cendron[1,10,*]

[1]Dipartimento di Biologia, Università degli Studi di Padova, Via Ugo Bassi 58/b, 35131 Padova, Italy
[2]Biozentrum, University of Basel, CH-4056 Basel, Switzerland
[3]Cellular and Molecular Microbiology (CM2), Faculté des Sciences, Université Libre de Bruxelles (ULB), 12 rue des Professeurs Jeener et Brachet, B-6041 Brussels, Belgium
[4]Dipartimento di Scienze Cliniche Applicate e Biotecnologiche, Università degli Studi dell'Aquila, Via Vetoio 1, 67100 L'Aquila, Italy
[5]Dipartimento di Scienze Biomediche, Università degli Studi di Padova, Via Ugo Bassi 58/b, 35131 Padova, Italy
[6]VIB-VUB Center for Structural Biology, Vrije Universiteit Brussel, Pleinlaan 2, 1050 Brussels, Belgium
[7]Dipartimento di Scienze Molecolari e Nanosistemi, Università Ca' Foscari Venezia, via Torino 155, 30172 Mestre, Venice, Italy
[8]Dipartimento di Scienze della Vita, Università degli Studi di Modena e Reggio Emilia, via Giuseppe Campi 103, 41125 Modena, Italy
[9]These authors contributed equally
[10]Lead contact
*Correspondence: laura.cendron@unipd.it
https://doi.org/10.1016/j.str.2022.09.004

SUMMARY

Antimicrobial resistance threatens the eradication of infectious diseases and impairs the efficacy of available therapeutics. The bacterial SOS pathway is a conserved response triggered by genotoxic stresses and represents one of the principal mechanisms that lead to resistance. The RecA recombinase acts as a DNA-damage sensor inducing the autoproteolysis of the transcriptional repressor LexA, thereby derepressing SOS genes that mediate DNA repair, survival to chemotherapy, and hypermutation. The inhibition of such pathway represents a promising strategy for delaying the evolution of antimicrobial resistance. We report the identification, via llama immunization and phage display, of nanobodies that bind LexA with sub-micromolar affinity and block autoproteolysis, repressing SOS response in *Escherichia coli*. Biophysical characterization of nanobody-LexA complexes revealed that they act by trapping LexA in an inactive conformation and interfering with RecA engagement. Our studies pave the way to the development of new-generation antibiotic adjuvants for the treatment of bacterial infections.

INTRODUCTION

The therapeutic success of modern medicine in eradicating infectious diseases as well as in surgical interventions and treatment of chronic diseases and cancer strictly relies on the availability of an efficacious antimicrobial arsenal. After half a century of successful control of bacterial infections, the intensive use and misuse of antibiotics from human to veterinary medicine and animal farming caused the emergence and spread of multidrug-resistant bacteria, which has become a global emergency in recent years (Appelbaum, 2012; ECDC, 2009; Nübel, 2016; Santajit and Indrawattana, 2016). The development of novel antimicrobial drugs implies costs that hardly achieve sustainability in view of their short administration times compared with chronic disease therapies and, most importantly, rapid evolution of antibiotic resistance, dramatically reducing the outcome of the antimicrobial treatment (Rice, 2008).

Bacterial exposure to genotoxic agents such as β-lactam (Miller et al., 2004), quinolone (Cirz et al., 2005, 2007), and aminoglycoside antibiotics activates the expression of stress-induced mutagenic pathways, among which the SOS response is one of the most characterized (Harms et al., 2016; Simmons et al., 2008). Discovered in the 1970s, it emerged as a near-universal response to DNA damage, present in almost all eubacterial groups, playing a central role in both favoring bacterial persistence and evolution of resistance (Blázquez et al., 2018; Cirz et al., 2007; Radman, 1975; Walter et al., 2014). The regulation of the SOS response depends on two proteins: the RecA recombinase and the bifunctional protein LexA, bearing both transcriptional repressor and autoproteolytic activities (Baharoglu and Mazel, 2014; Blázquez et al., 2018; Foti et al., 2010; Maslowska et al., 2019). As a consequence of DNA lesions, single-stranded DNA (ssDNA) accumulates and promotes ATP-dependent polymerization of RecA recombinase, a prerequisite of its activation

(ssDNA/RecA nucleoprotein complex, referred to as RecA*). Such nascent nucleoprotein complexes extend via oligomerization across thousands of nucleotides mediated by RecA core domain (Baharoglu and Mazel, 2014). RecA* promote LexA autocleavage, resulting in derepression of SOS-regulated genes. This sensor-effector mechanism tightly controls the timing and level of expression of a diverse array of genes involved in DNA exchange and repair, cell-division arrest, motility, biofilm formation, and vesiculation, with species-specific differences in the number and type of genes under LexA control (Giese et al., 2008; Mok and Brynildsen, 2018; Yeeles and Marians, 2013). *Escherichia coli recA* and *lexA* genes are under the control of the LexA transcriptional repression as well. This ensures a rapid shut-off of the SOS response after cessation of the genotoxic stress (Maslowska et al., 2019).

The LexA protein is composed of an N-terminal DNA-binding domain (NTD) and a C-terminal autoproteolytic domain (CTD). LexA forms homodimers through a dimerization interface present on the CTD. LexA dimers bind to specific target DNA sequences called SOS boxes via a classical N-terminal helix-turn-helix motif that engages both the major and the minor grooves of double-stranded DNA. SOS boxes are 20-bp imperfect palindromes present in SOS gene promoters. Binding of LexA to SOS boxes represses transcription of SOS genes at the promoter and blocks RNA polymerase activity (Zhang et al., 2010). Sequence variability of SOS boxes causes different binding strength by LexA and accordingly determines derepression timing and extent during SOS response (Culyba et al., 2018). LexA self-cleavage activity fully resides on its CTD: it is catalyzed by the highly conserved dyad K156/S119 and the hydrolyzed peptide bond locates between residues A84 and G85, situated within the loop 78–99 (the so-called cleavable loop). This loop is engaged in a conformational change from an open inactive state to an activated/prone-to-be-cleaved one, which is required for LexA autoproteolysis (Butala et al., 2009; Luo et al., 2001). The autocleavage separates the two LexA domains and promotes LexA dimer dissociation from the SOS boxes (Butala et al., 2009). X-ray structures of *E. coli* LexA (in the form of non-cleavable mutants) and RecA have been determined, allowing the description of the most relevant features of SOS response mechanism (Blázquez, 2003; Luo et al., 2001; Xing and Bell, 2004).

The gene network under SOS control includes DNA repair mechanisms, such as translesion synthesis over damaged DNA, catalyzed by error-prone DNA polymerases (Cirz et al., 2005; Foti et al., 2010; Maslowska et al., 2019). This increases bacterial evolvability and, in the presence of an antibiotic exerting a selective pressure, resistant variants will be selected (Blázquez et al., 2018; Cirz et al., 2005). Moreover, the SOS response can modulate the expression of integrases and transposases, which might facilitate horizontal gene transfer and the spreading of gene cassettes conferring antibiotic resistance within bacterial populations (Beaber et al., 2004; Boshoff et al., 2003; Chellappa et al., 2013; Fernández De Henestrosa et al., 2000; Strugeon et al., 2016).

Furthermore, SOS pathway activation controls TisB-IstR toxin-antitoxin system, reduces swimming motility and induces vesiculation as well as biofilm formation and maturation (Beaber et al., 2004; Chellappa et al., 2013; Jolivet-Gougeon and Bonnaure-Mallet, 2014; Recacha et al., 2019; Strugeon et al., 2016). *In vivo* experiments using neutropenic murine models of infection revealed that the increase in mutagenesis rate triggered by antimicrobials has a clear impact on resistance gain, behaving *de facto* as the driving force of bacterial adaptability (Alam et al., 2016; Cirz and Romesberg, 2007; Culyba et al., 2015). The inhibition or modulation of RecA or LexA has a direct effect on the expression of genes involved in the SOS response and on the development of intrinsic resistance and acquisition of antimicrobial resistance genes. The relevance of such a mechanism has been demonstrated in a murine model of infection with an *E. coli* strain carrying an uncleavable LexA mutant (LexA^{S119A}), where SOS response was abolished: the occurrence of resistant mutants under rifampicin treatment was impaired compared with control mice infected with wild-type (wt) *E. coli* (Cirz et al., 2005). Analogous results were obtained in a neutropenic mouse model of infection using RecA inhibitors (Alam et al., 2016).

The inhibition of RecA* directly affects LexA autocleavage and subsequent SOS response activation, theoretically supporting the possibility of developing an effective antibiotic adjuvant (Mo et al., 2016; Yu et al., 2001). To modulate SOS response, high-throughput screening approaches have been applied to target RecA ATPase activity. However, the high degree of sequence similarity of RecA with Rad51, a human drug target that plays a key role in DNA repair mechanisms during replication, emerged as a serious concern due to the high risk of off-target effects (Alam et al., 2016; Bellio et al., 2017, 2020; Nautiyal et al., 2014; Short et al., 2016; Tiwari et al., 2018; Wigle and Singleton, 2007; Xu et al., 2017; Yakimov et al., 2017). On the contrary, targeting LexA autoproteolysis, a reaction unique to the prokaryotic SOS response, would represent a valid possibility to selectively contrast bacterial infections. Recent evidence supports the efficacy of approaches targeting LexA repressor in fighting antibiotic resistance (Mo et al., 2018; Selwood et al., 2018).

LexA protease belongs to the serine proteases superfamily but carries structural and functional features distinct from prototypical serine proteases based on a catalytic triad. One of the biggest barriers to the development of LexA inhibitors is that it undergoes an intramolecular proteolytic cleavage, but cannot function in *trans* (Mo et al., 2014). This precludes high-throughput screening with oligopeptide substrates or canonical libraries, making it challenging to search for small-molecule inhibitors able to overcome the high apparent concentration of the preferred substrate (Culyba et al., 2015).

To address these barriers, we considered the use of nanobodies (Nbs) in light of their peculiar features: the capability to target conformational epitopes not accessible to conventional antibodies, providing a larger interaction surface that can lock LexA in an uncleavable conformation, as well as their demonstrated ability to bind and modulate the activity of both intracellular and extracellular targets with unprecedented potency and selectivity (Danquah et al., 2016; Errasti-Murugarren et al., 2019; Fumey et al., 2017). We produced and screened a library of llama-derived Nbs and discovered sub-micromolar binders of LexA (Figure 1A), which turned out to be the most potent ever reported inhibitors of LexA autoproteolysis both *in vitro* and in *E. coli* culture experiments. *In vitro* functional and

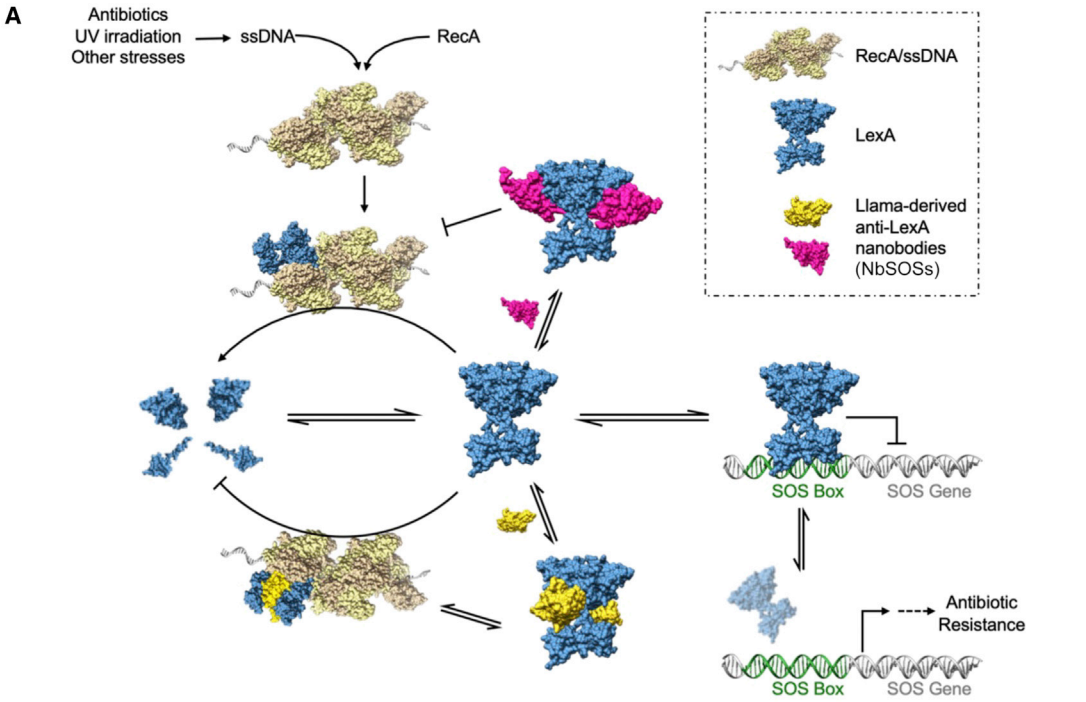

B

Nb	Nbs panning conditions		
	SOS complex (solid phase)	LexA S119A (neutravidin capture)	LexA 75-202 (G85D) (neutravidin capture)
NbSOS1	x	x	x
NbSOS2	x	x	x
NbSOS3	x	x	x
NbSOS4			
NbSOS5	x	x	
NbSOS6	x		
NbSOS7	x		
NbSOS8	x		
NbSOS9	x		

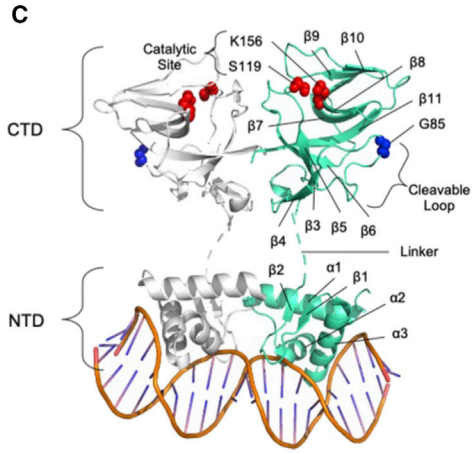

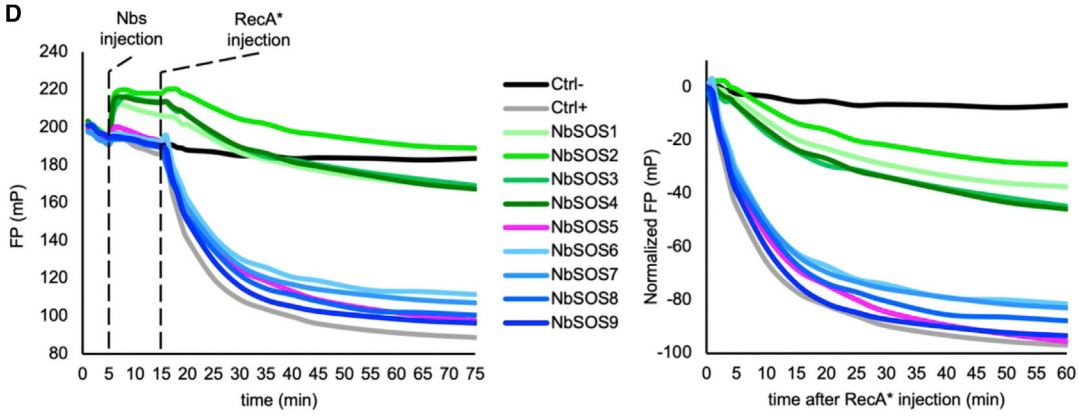

Figure 1. NbSOS candidates selection and preliminary inhibition screening versus LexA repressor autocleavage

(A) Scheme of the approach used in this study to target the SOS response: Nbs targeting *E. coli* SOS response system (NbSOSs) are developed to inhibit the RecA*-induced LexA autoproteolysis and keep repressed the downstream genes under LexA control. This inhibitory effect can be exerted by interfering with

(legend continued on next page)

structural studies shed light on the inhibition mechanism of the three most active Nbs and disclosed the structural determinants at the base of LexA inactivation and SOS response suppression. Our results offer the starting point for the design of novel molecules that might increase bacterial susceptibility to antimicrobials and, most importantly, reduce antibiotic-induced mutagenesis.

RESULTS

Generation and panning of Nbs against *E. coli* RecA*/LexA complex

In a campaign to develop Nbs targeting the components of *E. coli* SOS complex at different stages of the process, a llama was immunized with a recombinant mixture of *E. coli* LexA (wt) and LexA^{S119A}, in complex with RecA* and stabilized by crosslinking in mild conditions (Figures S1A and S1B). Peripheral blood lymphocytes were isolated, and total RNA was extracted and reverse transcribed to cDNA coding for Nbs. Using phage display technology (Pardon et al., 2014), Nbs were selected against solid-phase immobilized crosslinked antigen complexes, the neutravidin-captured biotinylated catalytically dead LexA^{S119A}, or the biotinylated uncleavable G85D mutant of LexA CTD (LexA$^{75\text{-}202(G85D)}$). Similar conditions were used for ELISA testing of enriched Nbs, from which a total of 124 unique Nb sequences were identified and divided into 30 families according to Complementary Determining Region 3 (CDR3) sequence similarity. Nine of them were selected for subsequent analysis (NbSOS1 to NbSOS9), chosen to cover the most diverse variants and taking into account specificity (as revealed by ELISA testing), family enrichment, and stringency of selection conditions (Figure 1B).

Nbs inhibit LexA autoproteolysis in the low micromolar range

To assess the ability of the nine selected NbSOSs to inhibit the LexA-RecA* axis, we used a fluorescence polarization (FP)-based LexA autoproteolysis assay (Mo et al., 2018). It relies on a recombinant LexA CTD (including both the catalytic dyad S119/K156 and the autocleavage site A84-G85; Figure 1C), bearing an N-terminal tetracysteine motif (CCPGCC) fluorescently labeled by the biarsenical FlAsH-EDT$_2$ reagent (FlAsH-LexA$^{75\text{-}202}$). In particular, NbSOS1, NbSOS2, and NbSOS3 inhibit RecA*-induced FlAsH-LexA$^{75\text{-}202}$ autoproteolysis with half maximal inhibitory concentration (IC_{50}) values ranging from 0.64 to 1.8 μM (Figures 1D and 2A; Table 1). The ability of these three NbSOSs to inhibit wt LexA was further examined by using an orthogonal assay based on SDS-PAGE and band densitometry analysis (Figure S1E). The determined IC_{50} values (0.6–2.2 μM) correlate well with those obtained using the FP-based assay (Figure 2B and Table 1).

To gain insight on NbSOSs' mechanism of action, the aforementioned FP setup was used to follow FlAsH-LexA$^{75\text{-}202}$ autoproteolysis induced by alkaline pH, as this condition is known to trigger the autocleavage reaction in a RecA*-independent manner (Slilaty et al., 1986). Notably, NbSOSs demonstrated to inhibit LexA autocleavage in a dose-dependent manner at pH 9, when the process is triggered only by basic pH (Figure 2C), suggesting inhibition activity is exerted directly on LexA.

Hence, we determined the binding affinities of NbSOSs to LexA by using two different methodologies: surface plasmon resonance (SPR), performed flowing NbSOSs on a chip-immobilized full-length LexA^{S119A} mutant (Figures 2D and 2E), and the FP-based assay described above (without challenging FlAsH-LexA$^{75\text{-}202}$ with RecA*), exploring increasing concentrations of Nbs (Figure 2F). In the SPR assay, where the more conservative full-length LexA^{S119A} has been used, all Nbs exhibited submicromolar binding affinities toward the antigen ($K_D \sim 0.2$ μM; Figure 2B; Table 1). Measured affinities have been confirmed by FP, with K_D values ranging between 0.05 and 0.10 μM (Figure 2F; Table 1). Overall, the experimental data suggest that three out of the nine NbSOSs studied have potent affinity and inhibitory properties toward LexA autoproteolytic activity. Among the characterized Nbs, we discovered that NbSOS2 has the greatest inhibitory potency on RecA*-induced LexA autocleavage.

LexA inhibition occurs via cleavable loop engagement in an inactive state

To better determine the molecular basis of LexA autoproteolysis inhibition by the Nbs, we solved the crystal structures of wt LexA in complex with NbSOS1, 2, and 3 (hereinafter referred to simply as *NbSOSs*; Figures 3, 4, and S3–S5; Table S3). X-rays revealed that all three NbSOSs recruit the CTD of LexA with a 2:2 stoichiometry, fully described in the crystal asymmetric unit. The Nbs did not make any contacts with the LexA NTD. Consistently with previously solved structures of full-length LexA (Luo et al., 2001), the NTD was not visible in the electron density maps, despite still being present in the crystallized construct (as demonstrated by SDS-PAGE analysis of crystals obtained in

RecA*-LexA binding (depicted as purple Nb) and/or by stabilizing LexA in an uncleavable conformation (but still permitting RecA*-LexA interaction; depicted as yellow Nb).

(B) NbSOSs screened in this work, chosen as representative members of distinct Nb families, grouped according to CDR3 sequence similarity. NbSOSs have been submitted to parallel selections against LexA-RecA* crosslinked complex (antigen-coated plates) or uncleavable mutant full-length LexA (LexA^{S119A}) and LexA CTD (LexA$^{75\text{-}202(G85D)}$), biotinylated and immobilized on neutravidin agarose beads.

(C) DNA-bound LexA dimeric structure where subdomains (NTD and CTD) and secondary structure elements (α1-3 and β1-11) are shown. Key residues on the cleavage loop (G85) and in the catalytic site (S119 and K156) are shown as blue and red spheres respectively; NTD-DNA structure was taken from PDB 3JSO and merged to CTD from PDB 7ZRA.

(D) Fluorescence polarization (FP) screening of selected NbSOSs to test their LexA autocleavage inhibition potential. The FP signal of FlAsH-LexA$^{75\text{-}202}$ alone was monitored for 5 min, then NbSOS was added and the FP measurement proceeded for 10 min before injecting RecA*. The full system (LexA:RecA:NbSOS molar ratio of 1:1:2) was assayed by FP for further 60 min. To account for FP increase due to NbSOS binding to LexA/RecA and avoid misleading inhibitory potential evaluation, curves were normalized by subtracting to each point the FP value right after RecA* injection (panel d, right). In blue, the behavior of NbSOSs selected only against the whole SOS complex antigen; in magenta, NbSOS5 targeting full-length LexA; in green, NbSOSs targeting specifically LexA CTD; in black and gray, the negative (LexA and buffer) and positive control (LexA + RecA*) reactions.

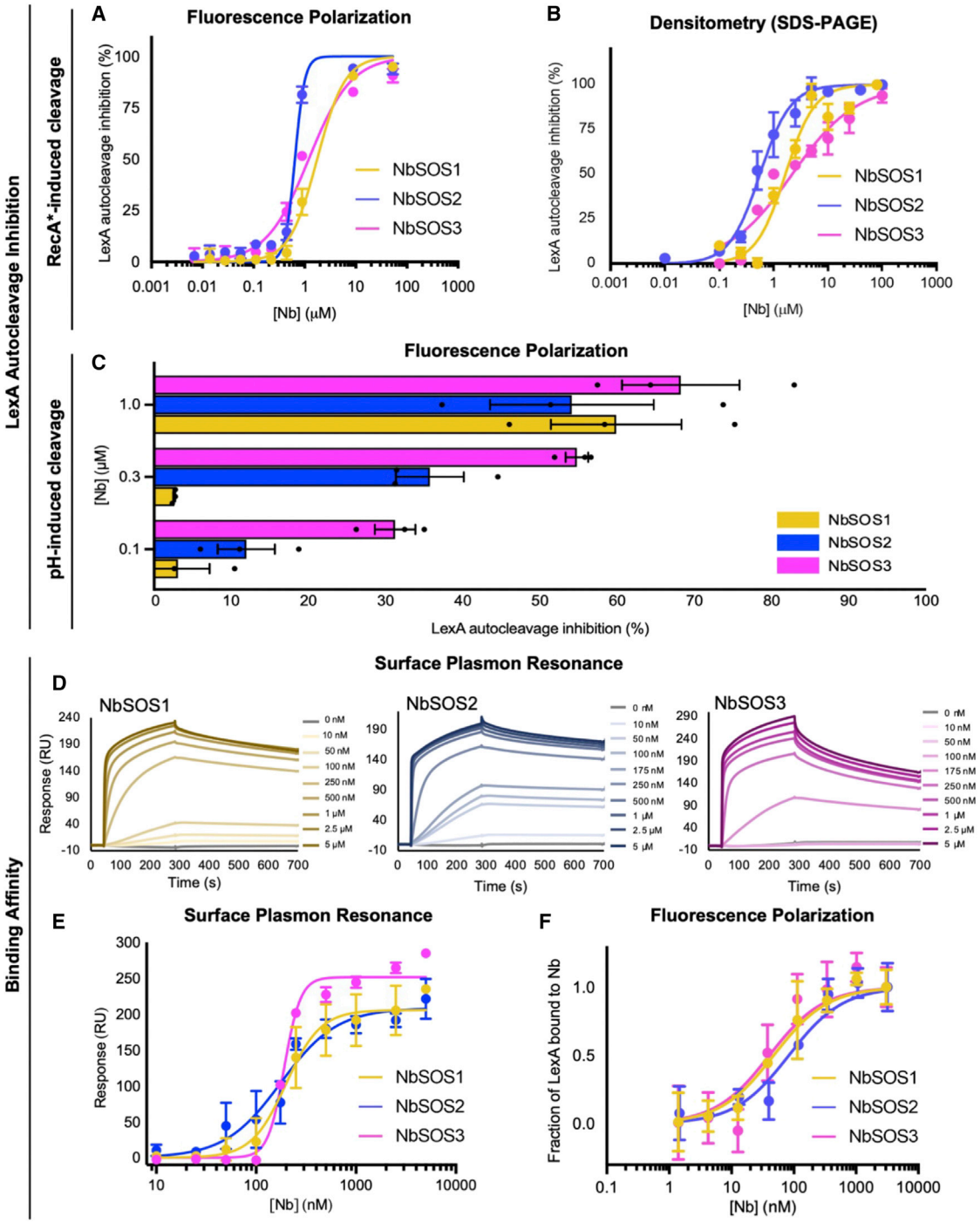

Figure 2. Biophysical characterization of NbSOS1, NbSOS2, and NbSOS3

(A and B) Inhibition of RecA*-induced LexA autocleavage by NbSOS1, 2, and 3 was evaluated by titrating the LexA/RecA* complex with NbSOSs and following LexA proteolysis by FP (panel a; FlAsH-LexA$^{75-202}$ is used) or SDS-PAGE band densitometry (panel b; LexA FL is used, see Figure S1E for representative SDS-PAGE gels used for IC_{50} measurement).

(C) Inhibition of alkaline pH-induced FlAsH-LexA$^{75-202}$ autocleavage by NbSOS1, 2 and 3, as measured by FP.

(D) Representative SPR sensorgrams showing binding kinetics of NbSOS1 (yellow, left), NbSOS2 (blue, center), and NbSOS3 (magenta, right) to immobilized LexA^{S119A}.

(E) Steady-state affinity analysis of SPR data.

(F) In-solution binding of NbSOSs to fluorescent FlAsH-LexA$^{75-202}$, evaluated by FP increase upon titration of FlAsH-LexA$^{75-202}$ with the 3 NbSOSs. All experimental points represent the average of three replicates. Error bars represent SD except in panel c, where the standard error of the mean (SEM) is reported. K_D and IC_{50} values obtained with the different techniques are reported in Table 1.

Table 1. Binding affinity (K_D) and IC_{50} values of the three selected NbSOSs

NbSOS	K_D (μM)		IC_{50} (μM)	
	SPR (LexA^{S119A})	FP (FlAsH-LexA$^{75-202}$)	SDS-PAGE (LexA)	FP (FlAsH-LexA$^{75-202}$)
NbSOS1	0.20 (0.15–0.28)	0.05 (0.03–0.09)	1.65 (1.11–2.50)	1.75 (1.30–2.16)
NbSOS2	0.18 (0.13–0.27)	0.08 (0.05–0.13)	0.56 (0.47–0.67)	0.64 (0.60–0.69)
NbSOS3	0.19 (0.18–0.21)	0.04 (0.02–0.09)	2.20 (1.26–3.96)	1.20 (0.90–1.60)

Measurements of K_D and IC_{50} values (with 95% confidence intervals in brackets) obtained with the highlighted methods were calculated by fitting curves reported in Figure 2, as described in the STAR Methods section.

the conditions of the diffracting ones; Figure S1D). Indeed, the model of LexA was traceable only from residues E71 (in complex with NbSOS3) and E74 (in complexes with NbSOS1 and 2). This finding suggests that the selected Nbs do not affect the conformational flexibility of the NTD domain in solution (Figure 1C). Although presenting highly diverse CDR3 loops in terms of charge and size, NbSOS1 and NbSOS2 share the same interaction surface and superpose very well in the complex (0.8 Å root-mean-square deviation [RMSD] over 110 Cα atoms, as calculated by Gesamt (Winn et al., 2011); Figure 4B) (Krissinel and Henrick, 2007). They trap dimeric LexA by contacting distinct CTD portions of both protomers at the same time (Figures 3, 4, and S3–S5): the cleavable loop of one LexA monomer and the cleavable loop hinge region of the adjacent one, fulfilling the crevice surface defined by the repressor dimerization region. As a result, the homodimer is seized up in an inactive state.

On the contrary, NbSOS3 binds a peripheral zone of each LexA CTD monomer, directly contacting the cleavage site of the loop and stabilizing it in a non-cleavable conformation (Figure 4B). Electrostatic interactions play a key role in NbSOS-LexA binding in the case of NbSOS1 and 2, while they are less pronounced for NbSOS3. As a matter of fact, NbSOS1 and NbSOS2 surfaces are characterized by a patch of positively charged residues that engage a heavily negative surface on the LexA counterpart, enriched in glutamates that belong to the hinge region, the cleavable loop arm, and the upstream fragment linking NTD and CTD (Figure S6). Positive surface potential at physiological pH is more pronounced for NbSOS2 than NbSOS1 (pI 9.26 and 7.84 respectively; Figure S6) and correlate well with their higher affinity toward LexA.

In more detail, NbSOS1 and NbSOS2 contact specific LexA stretches on both LexA protomers, namely cleavable loop arm residues 92–99 and C-terminal residues 199–202 of one LexA chain, and at the same time residues 101–108, belonging to the helical hinge at the base of the cleavable loop of the flanking LexA chain (Figure 4). Fragment 92–99 of the LexA cleavable loop, downstream from the cleavage site, forms a continuous β sheet with NbSOS1/2 CDR2 variable region (amino acids 52–59; Figures 3A, 4A, 4B, and S3) and the adjacent β strands, producing an uninterrupted concave sheet with the NbSOS1/2 backbone (β3c-β3b-β3-β6 and β37).

As calculated by PISA software (Krissinel and Henrick, 2007), the molecular surface of each NbSOS1/2 chain forming the LexA:NbSOS1/2 complex buries 1,000 and 1,100 Å^2, respectively, of which 619.7 Å^2 (NbSOS1) and 700 Å^2 (NbSOS2) upon interacting with one LexA protomer and contacting directly its cleavable loop, while the remaining 331.2 Å^2 (NbSOS1) and 400 Å^2 (NbSOS2) are engaged by the adjacent LexA protomer (Figure S8).

CDR2 and CDR3 regions contribute with the main binding paratopes to LexA-NbSOS1/2 complexes stabilization (Figures S3A and S3B). The main difference between NbSOS1 and 2 pertains CDR3 loop, much shorter and with a less acidic character in NbSOS2. CDR2 amino acids of NbSOS1/2, together with K96 of CDR3 (and R98 in the case of NbSOS1) further contact the C-terminal tail residues 201 and 202 of the same LexA monomer and favor its protrusion toward the concave surface of Nb β-backbone (Figures 4A, 4C, and S2B). Differently from apo structures, where the last residues of LexA are loose or point to the LexA dimerization surface, in our complexes the C-terminal segment appears largely engaged in an ordered network of hydrogen bonds and polar interactions with NbSOS1/2 CDRs. An extra salt bridge, peculiar to NbSOS2 CDR2 and involving its residue R58 and LexA D200, further strengthens the interaction between the Nb and LexA. The same bonding contact is prevented in NbSOS1, where Arg at position 58 is substituted by Asn, interrupting a pattern of alternate positive and negative charges peculiar to this interaction surface (Table S2). Finally, LexA helical motif 101–108, defining the cleavable loop hinge of the adjacent LexA monomer, is trapped by multiple polar and hydrogen bonds and two salt bridges by residues 52–56 of NbSOS1/2 CDR2, with the additional contribution of N32 from CDR1, R98 from CDR3 in the case of NbSOS1 and D103 from CDR3 in the NbSOS2 (Figures 4B, 4C, and S3).

While CDR2 and CDR3 interact the most with the antigen, few conserved residues belonging to NbSOS1 and NbSOS2 backbone are involved in antigen recognition (Figure S2B). Notably Y37, Y59, and G65 are all highly conserved among llama-derived Nbs: Y37 hydroxyl group forms hydrogen bonds with LexA chain A terminal residue L202, and Y59 and G65 main chain atoms are hydrogen bonded to LexA chain A residues E95 and Q91, respectively.

Conversely in the case of NbSOS3, CDR1 and CDR2 do not participate in LexA binding. Indeed, NbSOS3 flanks and blocks LexA mainly by few CDR3 residues and the long conserved loop between residues 39 and 47, within the Nb framework (Figures 4A and 4B). Three residues of the long beta-structured CDR3 contact LexA by hydrogen bonds: Y102 and R103 interact with LexA residues E71 and G75 respectively, while S110 hydrogen bonds with G85 carboxyl group in the LexA cleavage site and with R148 and D150 in the LexA loop connecting β strands β7 to β8 (Figure S5). Further weak non-bonded contacts involve CDR3, within residues 99 and 110.

To further support the significance of the interactions observed in the crystallized complexes, we tested the affinity of NbSOSs toward full-length LexA^{G85D} inactive mutant by SPR, in the same conditions reported above for LexA^{S119A}. As

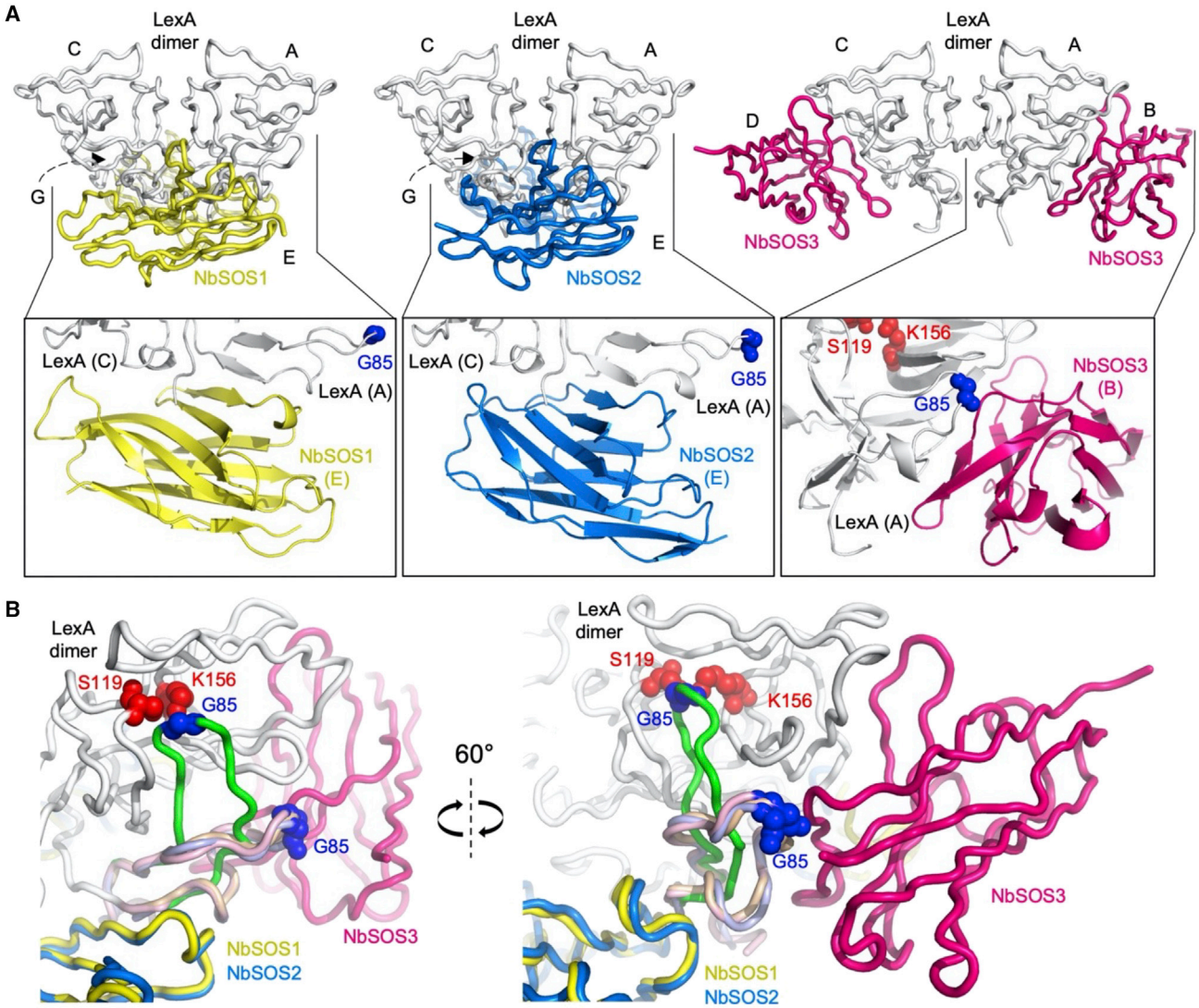

Figure 3. Structural basis of LexA autocleavage inhibition by NbSOSs binding

(A and B) Upper part: tube representation of crystal structures of LexA dimers (chains A and C) in complex with the three binders NbSOSs (chains E and G, B and D). Left: LexA (white), NbSOS1 (yellow), PDB 7ZRA; center, LexA (white), NbSOS2 (marine blue), PDB 7OCJ; right, LexA (white), NbSOS3 (hot pink), PDB 7B5G. For both NbSOS1 and NbSOS2, chain E is oriented toward the front, while chain G is on the back, indicated by a dashed arrow. Lower part: detailed cartoon representation of NbSOS1, 2, and 3 regions interacting with LexA. Red spheres indicate atoms of residues S119 and K156 of LexA catalytic dyad, while blue spheres represent G85 of LexA cleavage site. It is noteworthy that all the three NbSOSs bind a portion of LexA cleavable loop, defining, in the case of NbSOS1 and 2, a unique continuous β sheet. This critical detail is further underlined in panel b, where two magnified orientations (rotated by 60°) of cleavage site and loop region are shown. LexA cleavable loop structure of LexA-NbSOS1 (NbSOS1 in yellow, LexA cleavable loop in wheat), LexA-NbSOS2 (NbSOS2 in marine blue, LexA cleavable loop in light blue), LexA-NbSOS3 (NbSOS3 in hot pink, LexA in white and its cleavable loop in light pink) are superimposed to its conformation in the LexA hyper-cleavable mutant (PDB: 1JHE; LexA cleavable loop in green). As for panel a, LexA key residues are shown as spheres: active site residues S119 and K156 in red and cleavage site G85 in blue. NbSOSs contact LexA cleavable loop preventing its entering into the catalytic site and thus impairing its cleavage.

shown by the recorded sensorgrams (Figure S7A), the mutation introduced in the cleavable loop worsened the affinity in all cases, with a major impact on the dissociation rate constants of the three NbSOSs.

Nb inhibitors compete with RecA* but not with DNA for binding to LexA

Electrophoretic mobility shift assay (EMSA), SPR, and FP assays were set up to evaluate NbSOSs' effect on LexA activities regulating the SOS response, namely SOS-box DNA binding (a property needed for LexA to keep SOS genes repressed) and interaction with RecA* (the event that triggers LexA autoproteolysis and SOS derepression). EMSA (Zhang et al., 2010) and SPR assay were used to assess the potential interference by NbSOSs with the binding of SOS-box DNA to LexA. Conversely, an FP assay relying on a S119A uncleavable variant of FlAsH-LexA$^{75\text{-}202}$ was exploited to evaluate the interference of NbSOSs on LexA-RecA* interaction.

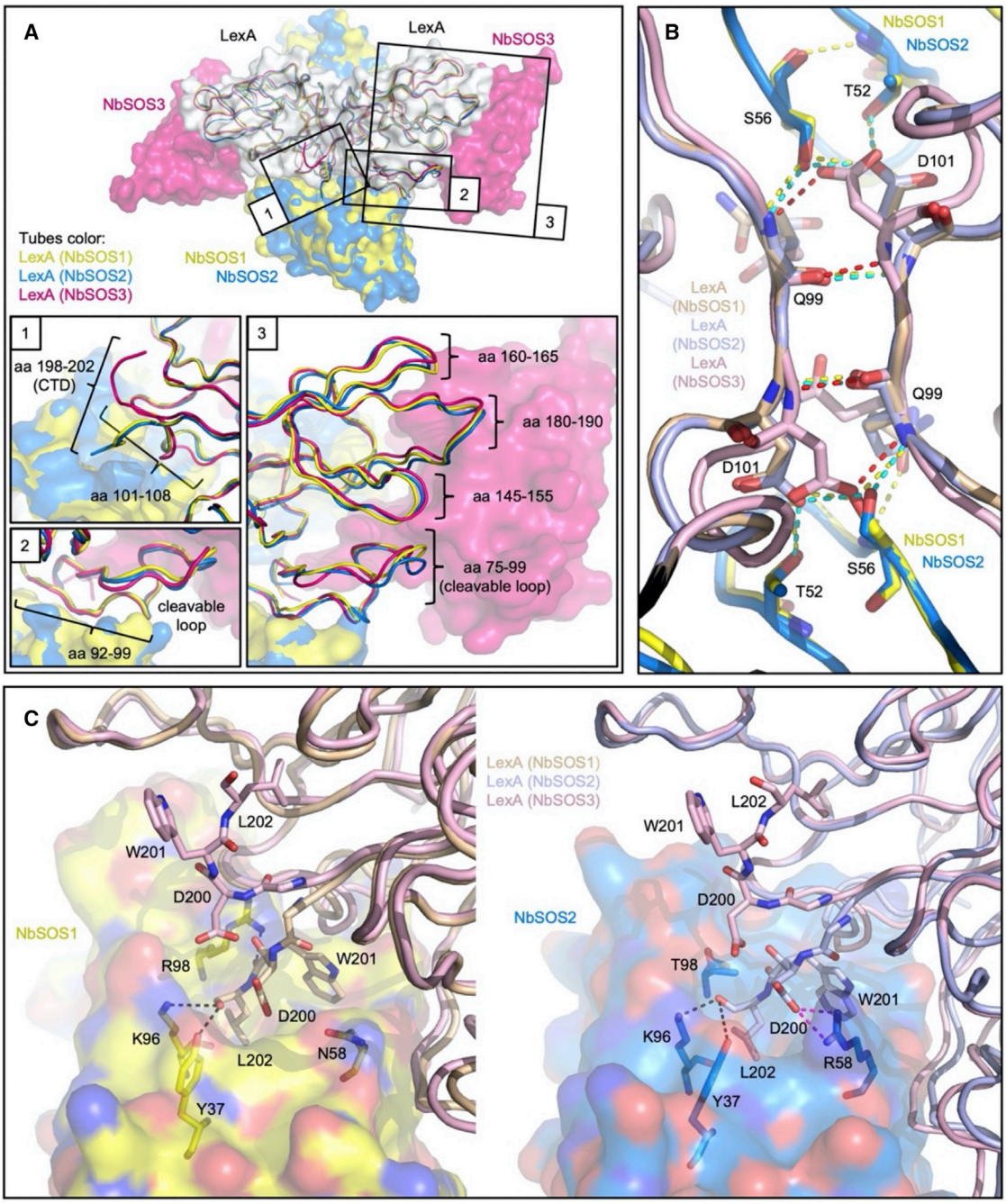

Figure 4. Details of LexA regions involved in NbSOS1-3 binding

(A) Mapping, on LexA-NbSOSs structure superimposition, of LexA regions engaged when binding different Nbs. Superimposed LexAs are depicted as tubes and Nbs as semi-transparent surfaces (yellow for LexA-NbSOS1, marine blue for LexA-NbSOS2, and hot pink for LexA-NbSOS3). Magnifications of interaction areas are framed in black.

(B) Magnification of a portion of LexA dimer (bottom of its CTD) that gets perturbed when contacted by NbSOS1 and 2 (compared with NbSOS3 or in absence of Nbs; the latter not shown). In this last panel, NbSOS1 and 2 are colored yellow and marine respectively, while LexA of LexA-NbSOS1 is colored wheat, LexA of LexA-NbSOS2 is colored light blue, and LexA of LexA-NbSOS3 is colored light pink.

(C) Magnification of LexA CTD when binding NbSOS3, compared with LexA-NbSOS1 (left) or LexA-NbSOS2 (right). When binding NbSOS1 or NbSOS2, LexA C-terminal gets trapped into a Nb pocket, thus being moved more than 10 Å away with respect to its position when binding NbSOS3 (which does not bind this LexA region). A relevant difference between NbSOS1 and NbSOS2 is the presence of the positively charged residue R58 in NbSOS2, substituted by uncharged N58 in NbSOS1: only in the former case a salt bridge is established with LexA D200. Hydrogen bonds are depicted as dashed black lines, salt bridges as dashed green lines.

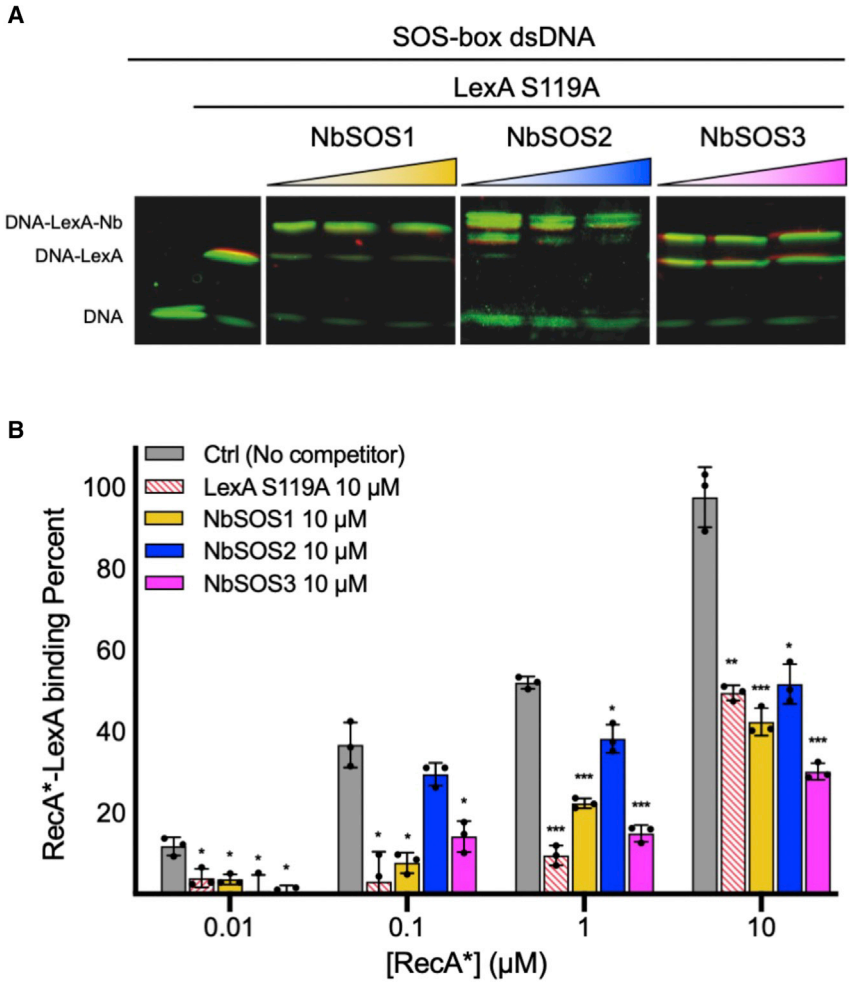

Figure 5. Investigations on NbSOSs interference with LexA-DNA and LexA-RecA* interactions

(A) EMSA depicting the electrophoretic mobility shift of SOS-box DNA upon binding by LexA and the supershift that characterizes DNA-LexA-NbSOS complexes. The 100 nM SOS-box dsDNA was incubated with 8 µM $LexA^{S119A}$ and 8, 24, or 48 µM NbSOS.

(B) FP-based RecA*-LexA binding assay. FlAsH-$LexA^{75\text{-}202\ (S119A)}$ was incubated with different concentrations of RecA*, either in the absence (Ctrl) or in the presence of investigated putative competitors of LexA-RecA* interaction. Unlabeled full-length $LexA^{S119A}$ (red dashed bars) was used to validate the ability of the assay to identify binding competitors. Means of three replicates are plotted, with error bars representing SD. Samples were compared with Ctrl treated with the same [RecA*] by t tests: *p < 0.03, **p < 0.002, ***p < 0.001.

In a pilot SPR assay, we determined *in vitro* a K_D of about 80 nM between the chosen SOS-box dsDNA and $LexA^{S119A}$ (Figure S7B), which approximates the previously estimated cellular concentration of SOS operator sequences in *E. coli* (~100 nM; Butala et al., 2011).

The EMSA was performed saturating SOS-box DNA (100 nM) with $LexA^{S119A}$ (8 µM), either alone or pre-incubated with an equimolar amount, a 3-fold or a 6-fold excess of each NbSOS, separately. In all the tested conditions, the addition of NbSOSs to LexA/SOS-box complex induces a band shift to a higher molecular weight (in agreement with a 2:2:1 Nb:LexA:SOS-box stoichiometry) compared with samples including only DNA and LexA, thus demonstrating that NbSOSs do not prevent LexA-DNA binding at transcriptional repressor sites (Figure 5A).

This observation is further sustained by SPR experiments in which chip-immobilized SOS-box DNA was first loaded with $LexA^{S119A}$ (100 nM), then fluxed by buffer solution for 600 s and finally challenged by saturating the chip with NbSOSs (0.1 - 2 µM). The final response clearly indicated the formation of DNA-LexA-NbSOS complexes (Figure S7C) and closely approaches the maximal response (ΔR_{NbSOS}) expected in the tested conditions (see equation below; Stevenson et al., 2021), demonstrating that none of the NbSOSs could displace the interaction between LexA and SOS-box DNA fragments.

$$\Delta R_{NbSOS} = R_{LexA} \times \frac{MW_{NbSOS}}{MW_{LexA}}$$

To test the ability of NbSOSs to interfere with RecA* binding to LexA, an uncleavable FlAsH-$LexA^{75\text{-}202\ (S119A)}$ construct was designed and produced. The assay was performed by FP measurements incubating 0.2 µM FlAsH-$LexA^{75\text{-}202\ (S119A)}$ with a 50-fold molar excess of each NbSOS, at different RecA* concentrations (1:20, 1:2, 5:1, 50:1 RecA*:FlAsH-$LexA^{75\text{-}202\ (S119A)}$). In all the tested conditions, samples including NbSOSs showed a reduced RecA*-LexA binding level compared with control reactions, with NbSOS3 exerting the highest competition (Figure 5B). The robustness of the assay was validated by a series of samples including an excess of unlabeled full-length $LexA^{S119A}$, which can compete with the fluorescently labeled LexA CTD for binding RecA* (Hostetler et al., 2020). These results suggest that NbSOSs can inhibit RecA*-induced LexA autocleavage not only by trapping its cleavable loop in an inactive conformation (as already discussed above) but also by interfering with the

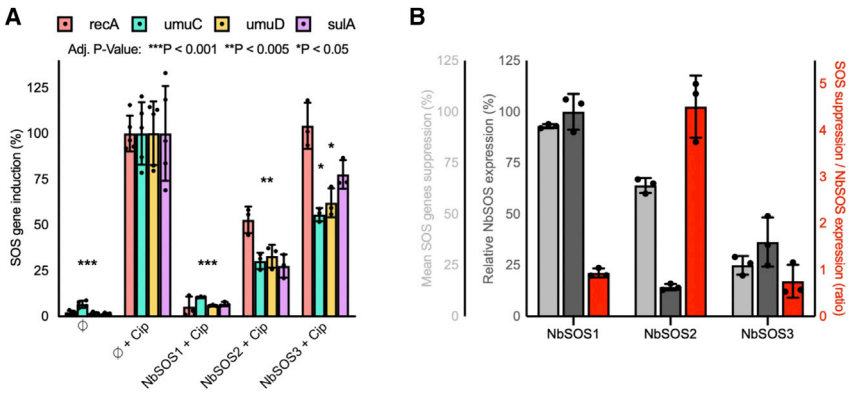

Figure 6. Expression profiling of SOS genes in the presence of NbSOSs

(A) *In vivo* SOS genes induction measured by RT-qPCR. For each reported SOS gene (*recA*, *umuC*, *umuD*, and *sulA*), 100% induction is represented by the average gene expression of samples treated with ciprofloxacin and containing empty pRham vector (*Ø + Cip*). *Ø* stands for samples containing empty pRham vector and not treated with ciprofloxacin. Samples expressing the three NbSOSs and treated with ciprofloxacin are referred to as *NbSOS1 + Cip*, *NbSOS2 + Cip*, and *NbSOS3 + Cip*. At least three biological replicates were analyzed for each sample (Ø, n = 4; Ø + Cip, n = 5; NbSOS1 + Cip, NbSOS2 + Cip, and NbSOS3 + Cip, n = 3). Error bars represent SD. Two-way ANOVA testing of the whole dataset confirmed that the main source of variation is among the conditions tested (>90% of total variation). Multiple t tests with Holm-Sidak correction were performed comparing all the conditions with ∅ + Cip, gene by gene. For conditions ∅, NbSOS1 + Cip, and NbSOS2 + Cip, a single p value is represented on the graph, since all the comparisons gave the same statistical significance. For NbSOS3 the p value is reported just for the genes that were significantly differently expressed compared with the control. Multiple t tests were performed also between NbSOS1 + Cip and NbSOS2 + Cip (resulting in significant difference, $p < 0.005$), NbSOS3 + Cip and NbSOS1 + Cip ($p < 0.001$), NbSOS3 + Cip and NbSOS2 + Cip ($p < 0.01$).

(B) SOS genes suppression relative to NbSOS expression. Plotted here together: in light gray bars, the average NbSOS-induced percent suppression of SOS genes monitored in this study (*recA*, *umuC*, *umuD*, and *sulA*; see values in Figure S8C); in dark gray bars, NbSOS expression levels in samples exploited for SOS genes expression analysis (measured by western blot analysis and normalized on NbSOS1, see also Figure S8B); in red bars, the ratio between average SOS genes suppression and NbSOS expression level. Error bars represent SD of three replicates (shown as black points).

binding event that triggers the conformational variation needed for autoproteolysis.

NbSOSs inhibit SOS response in *E. coli*

Given the promising results from *in vitro* LexA-inhibition assays, we tested the effect of the NbSOSs on the induction of the SOS response by DNA damaging antimicrobials in *E. coli*. With this aim, we performed RT-qPCR expression analysis of hallmark genes of the prototypical SOS pathway, in response to fluoroquinolone-induced DNA damage. Assayed genes included *recA*, *sulA* (coding for a factor involved in cell-division arrest), and the DNA-polymerase V encoding genes (*umuC* and *umuD*). To efficiently control the protein expression level, we cloned each NbSOS CDS in a plasmid containing a rhamnose-inducible promoter (pRham-NbSOSs). *E. coli* ATCC 25922 strains carrying either the pRham-NbSOSs or the empty vector (pRham∅) were subjected to ciprofloxacin treatment, or no treatment in the control cultures (Figures 6A and S8A). All the three NbSOSs displayed inhibitory activity toward SOS genes expression under ciprofloxacin stimuli, although with different levels of efficacy (Figure 6A). In the case of NbSOS1, the expression of the SOS genes in the presence of ciprofloxacin is comparable to the one measured in the untreated control, showing that NbSOS1 is a potent inhibitor of the SOS response in *E. coli*. We also normalized SOS genes suppression on the expression level of NbSOSs, as quantified by western blot on the same bacterial samples (Figures 6B, S8B, and S8C). These analyses clearly indicate a more stable and sustained expression level of NbSOS1 within the first 3 h of DNA stress by ciprofloxacin, while very low and unstable levels were observed in the case of NbSOS2 and NbSOS3. Interestingly, when normalized on Nb expression, the inhibitory effect on SOS response activation results more relevant for NbSOS2.

In the same conditions used for hallmark SOS genes profiling by RT-qPCR, the expression level of LexA repressor was monitored by western blotting technique, using an anti-LexA primary antibody (Figure S8D). The obtained results clearly indicate that all the NbSOSs can stabilize full-length LexA level up to 5 h after DNA-damage induction by ciprofloxacin, preventing its autoproteolysis. Conversely, full-length LexA in the control strain not expressing NbSOSs (*E. coli* ATCC 25922/pRham∅) rapidly disappears after fluoroquinolone treatment.

Considering that NbSOS1 showed a stronger expression level, it has been chosen as the best candidate for further analyses. To investigate its inhibitory role, we determined SOS induction inhibition at the single-cell level using a reporter gene assay based on an *E. coli* strain carrying a genome-integrated transcriptional fusion between the LexA-regulated *sulA* promoter and the *gfp* gene (*psulA::gfp*; strain SMR6669), previously shown to be a sensitive and specific reporter for the induction of the SOS response in live bacterial cells (Goormaghtigh and Van Melderen, 2019; Singletary et al., 2009). GFP fluorescence of *E. coli* SMR6669 cells transformed with either pRham-NbSOS1 or pRham∅ was measured under 60xMIC ofloxacin concentration, to induce the SOS system, and compared with non-treated cultures. These data show that, upon fluoroquinolone-induced DNA damage, a clear reduction of fluorescence occurs in the strain expressing NbSOS1 compared to the control strain (9-fold versus about 29-fold fluorescence increase following ofloxacin treatment), confirming that SOS response is repressed when this Nb is present (Figure 7A). However, the detected inhibition by NbSOS1 was not sufficient to produce either a consistent decrease of the cell survival rate in the tested cultures (Figure S9A) or an increase of antimicrobial susceptibility to ciprofloxacin (minimum inhibitory concentration, MIC), when comparing ATCC 25992 *E. coli* strain carrying pRham∅ (MIC 0.05 ± 0.03 μg/mL) with pRham-NbSOS1 (MIC 0.06 ± 0.04 μg/mL; Figure S9B). Finally, we analyzed SOS-induced, SulA-mediated *E. coli* filamentation under mild stress conditions (0.0078 μg/mL ciprofloxacin; 1/8 MIC) by DAPI whole-cell staining, using *E. coli* ATCC 25922 cells expressing NbSOS1 compared with the corresponding control strains (either *E. coli* ATCC 25992 wt or bearing pRham∅ vector). The filamentation induced by ciprofloxacin was strongly

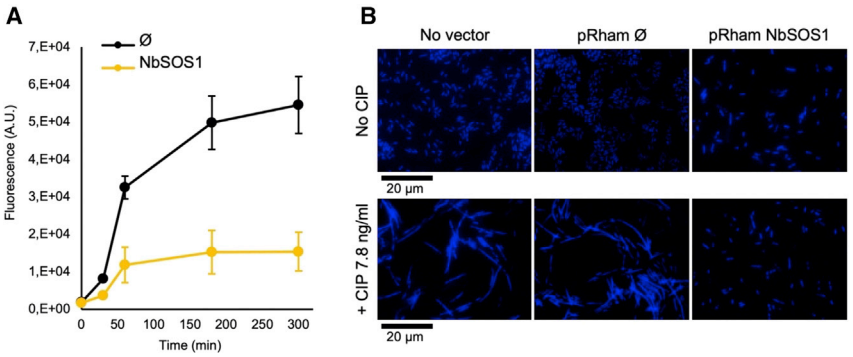

Figure 7. *In vivo* effects of NbSOSs on SOS response markers

(A) SOS response induced by ofloxacin treatment (5 μg/mL) in the presence or absence (Ø) of NbSOS1 expression, followed by the fluorescence emitted by an SOS-regulated GFP (*psulA:gfp* reporter construct). Five replicates were realized for this assay and error bars represent SD. (B) SOS-induced bacterial filamentation assessed by fluorescence microscopy (DAPI staining). Bacterial filamentation was evaluated on *E. coli* ATCC 25922 cells in absence (upper row) or presence (lower row) of antibiotic stress (0.0078 μg/mL ciprofloxacin). The experiment was carried out on untransformed *E. coli* cells (no vector, left column) and on bacteria transformed with either empty pRham vector (pRhamØ, center column) or pRham-NbSOS1 vector (right column). Filamentation is evident in both samples treated with ciprofloxacin that are not expressing NbSOS1 (no vector and pRhamØ), while no filamentation can be observed in untreated samples and in ciprofloxacin-treated sample expressing NbSOS1.

inhibited in the presence of NbSOS1 compared to the control strain: indeed, upon ciprofloxacin treatment, while a clear induction of filamentation is observed in wt and control strains, the resulting phenotype of *E. coli* ATCC 25922 cells expressing NbSOS1 recapitulates the features of *E. coli* in no-stress condition (Figure 7B). Taken together, these results demonstrated that NbSOS1 can inhibit SOS genes expression within bacterial cells by preventing LexA autoproteolysis.

DISCUSSION

In bacteria, the RecA/LexA axis of the SOS response represents a validated and promising drug target to fight antimicrobial resistance. Its suppression could extend the usability of current antimicrobial drugs and, under certain conditions, even rehabilitate in therapy available antibiotics that have become ineffective. With the purpose of modulating SOS response by exploiting novel routes of inhibition of RecA-stimulated LexA autoproteolysis, we isolated and characterized llama-derived Nbs raised against the LexA-RecA* complex, here renamed NbSOSs. Our approach led to the selection of three NbSOSs interfering with LexA autoproteolysis, whose biochemical and biophysical characterization revealed high-nanomolar to low-micromolar binding affinities and inhibitory potencies toward LexA (Figures 1 and 2; Table 1). More importantly, the selected NbSOSs do not prevent LexA binding activity toward SOS-box prototypical DNA sequence, which is needed to exert the physiological function of SOS repressor *in vivo* (Figure 5A).

Given the highly dynamic nature of LexA cleavage loop and the difficulty of targeting LexA with inhibitor molecules (Mo et al., 2014), crystal structures of the three most promising NbSOSs bound to LexA dimers not only shed light on NbSOSs mechanism of inhibition but also offer an opportunity for the rational design of both proteins and small molecules mimicking NbSOSs key features of interaction with LexA. The identified NbSOSs prevent LexA autoproteolysis by blocking its cleavable loop in an inactive state. As reported in previous structural studies (Luo et al., 2001; Zhang et al., 2010), the cleavable loop is characterized by a high flexibility (resulting partially undefined in several available structures; e.g., PDB 3JSO, 3JSP, 1JHF, and 1JHH), which accounts for its ability to fold either in a "cleavable state," placing the cleavage site close to the catalytic dyad S119-K156 (see e.g., PDB 1JHE and 3JSO), or in an inactive "open" state, where the cleavage site is located about 20 Å apart from the catalytic pocket (Zhang et al., 2010) (see e.g., PDB 1JHC and 3JSP). The latter conformation closely resembles the one observed in our complexes with NbSOSs. None of the selected NbSOSs recruit the LexA N-terminal domain, which, similarly to previously described LexA full-length X-ray structures, remains undefined (Luo et al., 2001).

Despite presenting highly diverse CDR3 loops, NbSOS1 and NbSOS2 explore the same interaction surface and superpose very well in the complexes with the LexA antigen (Figures 3 and 4). Intriguingly, a similarity can be found in the binding of gp7 protein, a bacteriophage GIL01 factor known to interact with LexA and able to increase the repressor affinity toward DNA SOS boxes, ultimately promoting lysogeny *in vivo* (Fornelos et al., 2015). It has been recently hypothesized that gp7 protein binds as a dimer to the LexA linker loop, contacting the CTD domain in a region overlapping the one explored by NbSOS1 and NbSOS2 (Caveney et al., 2019).

Conversely, even though LexA-inhibition mechanism of NbSOS3 relies on cleavable loop blockade as well, it explores a different LexA surface, largely peripheral, where the electrostatic contribution is less relevant than in the case of NbSOS1 and NbSOS2. Indeed, NbSOS3 still contacts a segment of the cleavable loop through polar and hydrogen bonds, interacting with amino acids positioned right after the cleavage site, but does not form the strong pattern of salt bridges and hydrogen bonds that sustains NbSOS1 and NbSOS2 affinity.

If the driving role of LexA cleavable loop blockade is supported by the capacity of NbSOSs to inhibit LexA even when the autoproteolysis is solely promoted by alkaline pH (Figure 2F), a further contribution to inhibition might be ascribed to NbSOSs interference with LexA-RecA* binding as observed in FP measurements, in particular in the case of NbSOS3 (Figure 6B).

When tested *in vivo* under genotoxic stress conditions by high doses of ciprofloxacin, all three NbSOSs significantly suppressed the expression of relevant SOS genes, although to a different extent. Indeed, our RT-qPCR analysis showed a strong reduction of *umu*D/C, *sul*A, and *rec*A mRNA levels in *E. coli* cultures expressing the Nbs, compared to the Nb-devoid controls. The most significant suppression was achieved in the presence of NbSOS1, reaching SOS genes expression levels comparable with no-stress conditions (Figure 6A). Such stronger

performance of NbSOS1 is justified by its higher expression and consequent concentration in the cytoplasm (Figure S8C). In agreement with what is observed *in vitro*, we reason that, if the inhibitory activity is normalized by the Nb expression level, NbSOS2 could offer an even stronger inhibitory performance, representing a promising candidate for future optimization studies (Figures 6B, S8C, and S8D).

The RT-qPCR results were confirmed by monitoring the induction of the SOS response using an *E. coli* strain harboring an SOS-regulated fluorescent reporter (*psulA::gfp*) and bearing a NbSOS1-coding plasmid vector. Under ofloxacin-induced stress conditions and in the presence of NbSOS1, we observed a 70% reduction of the maximal fluorescence signal, compared to the control (Figure 7A). DAPI whole-cell staining used to follow bacterial filamentation — observed after DNA damage induced by ciprofloxacin treatment and resulting from transient cell-division arrest via *sul*A overexpression and consequent FtsZ inhibition (Bellio et al., 2020) — further confirmed the SOS inhibitory activity of NbSOS1 *in vivo*. Indeed, the filamentous phenotype was clearly inhibited in the strain expressing NbSOS1 in the tested conditions (Figure 7B).

The SOS-response reduction exerted by NbSOS1 was robust but not yet sufficient to produce a corresponding decrease of the bacterial survival rate, nor an effect on ciprofloxacin MIC values (Figure S9). We expect that a cell survival impairment and a synergistic effect with antibiotics could be achieved with increased affinities and improved IC_{50} values toward LexA antigen. Strikingly results on antibiotic-mediated killing, bacterial persistence, biofilm formation, and resistance onset were obtained by delivering an uncleavable LexA mutant using bacteriophages (Lu and Collins, 2009), thus we reason that a similar LexA sequestration approach could be mimicked by our NbSOSs, once optimized. Our encouraging results will drive future Nb optimization in terms of affinity and stability but also sustain the screening or rational design of cell-permeable small molecules targeting LexA cleavable loop inactivation (Pardon et al., 2018).

To summarize, we reported a panel of Nbs active as strong inhibitors of LexA autoproteolysis, behaving as antagonists of SOS response in *E. coli* cultures. We detailed by X-ray crystallography their interactions with LexA, thus defining the premises for the development of SOS response inhibitors as future therapeutic adjuvants in antibiotic treatment.

SIGNIFICANCE

The effectiveness of currently available antimicrobial agents is being progressively hampered by the evolution of novel resistance mechanisms by bacterial pathogens, thus requiring priority research efforts. The bacterial SOS response to DNA damage represents one of the crucial pathways involved in antimicrobial resistance acquisition and is orchestrated mainly by the transcriptional repressor LexA and the RecA recombinase/DNA damage sensor. As reported in previous studies, the suppression of the SOS pathway (obtained by deletion or inactivating mutations on RecA or LexA) might be a feasible strategy to delay drug resistance onset and even to re-sensitize resistant microbes. This notwithstanding, currently known inhibitors of the RecA-LexA axis are limited to very few compounds, none of which have gained clinical applicability yet.

Fragments from camelid-derived heavy-chain-only antibodies (Nbs) are a promising biotechnological tool, characterized by low molecular dimensions (14–16 kDa), high tissue penetration, low immunogenicity in humans, notable stability, and easy production as recombinant proteins. In this work we have reported the selection, via llama immunization and phage display technology, of three anti-LexA Nbs (NbSOSs). Deep *in vitro* biochemical characterization demonstrated that NbSOSs are able to bind *E. coli* LexA with an unprecedented affinity and to inhibit its crucial autoproteolytic activity (required for the activation of SOS response), without precluding LexA binding to DNA.

SOS response inhibition by NbSOSs has been validated by several assays (SOS genes expression profiling by RT-qPCR, reporter gene assay, and phenotypic observation) on *E. coli* cultures treated with a common DNA damaging antibiotic.

X-ray structures of NbSOSs in complex with LexA revealed that they contact the target antigen in proximity of its cleavable loop, preventing the conformational change required for LexA autoproteolysis, while FP analysis disclosed interfering properties on RecA*-LexA engagement. Even though they need further advancement, the Nbs described in this study have the potential to become novel antibiotic adjuvants to be used in antimicrobial chemotherapy.

STAR★METHODS

Detailed methods are provided in the online version of this paper and include the following:

- KEY RESOURCES TABLE
- RESOURCE AVAILABILITY
  - Lead contact
  - Materials availability
  - Data and code availability
- EXPERIMENTAL MODEL AND SUBJECT DETAILS
  - Animals
  - Microbe strains
- METHOD DETAILS
  - Recombinant genes cloning and mutagenesis
  - Protein expression and purification
  - RecA activation
  - Antigen preparation, llama immunization and nanobodies discovery
  - Fluorescence polarization assays
  - SDS-PAGE LexA autocleavage assay
  - Surface Plasmon Resonance
  - Gene expression analysis by Real-time quantitative PCR (RT-qPCR)
  - Western blotting
  - Electrophoretic Mobility Shift Assay
  - Crystallization, data collection, structure determination and analysis
  - Fluorescent analysis of the SOS response induction
  - Cell survival assay
  - Filamentation assay
  - MIC determination
- QUANTIFICATION AND STATISTICAL ANALYSIS

SUPPLEMENTAL INFORMATION

Supplemental information can be found online at https://doi.org/10.1016/j.str.2022.09.004.

ACKNOWLEDGMENTS

This work was supported by Fondazione Cassa di Risparmio di Padova e Rovigo (grant number 2018/0557 and Cariparo PhD Grant program 2019) and University of Padova, Department of Biology (Post-Doctoral Grant Program). We acknowledge Instruct-ERIC (European Research Infrastructure in Structural Biology) for funding contribution (Nb4Instruct workshop, grant number PID6440) and the Research Foundation - Flanders (FWO) for their support for Nb discovery. We further acknowledge Nele Buys, Eva Beke, Katleen Willibal, and Allison Lundqvist for the technical assistance during Nb discovery and the Nb workshop. We would like to thank Diamond Light Source (MX21741) and the staff of beamline I04, the European Synchrotron Radiation Facility (ESRF, Grenoble, France) and the staff of beamline ID30A-1, as well as the beamline X06DA (PXIII) of the Swiss Light Source (SLS), Paul Scherrer Institut (Villigen, Switzerland) for provision of synchrotron radiation beamtime and for assistance during X-ray data collections. The graphical abstract was partly created with BioRender.com.

AUTHOR CONTRIBUTIONS

L.C., L.M., M.C., F.V., and D.T., conceived and designed the experiments. L.M., E.P., and M.C. produced and screened Nb libraries *in vitro*. L.M., F.V., and M.C. crystallized and solved complexes crystal structures. L.M., M.C., F.V., and E.C. performed DNA binding assays and SOS gene expression profiling in *E. coli* cultures. P.B. performed filamentation assays. F.G. performed fluorescent analysis of the SOS response induction. L.M., F.V., and M.R. performed SPR measurements. L.C., D.T., A.A., G.C., J.S., and L.V.M. wrote the paper. All authors critically discussed the results and commented on the paper.

DECLARATION OF INTERESTS

The authors declare no competing interests.

Received: December 30, 2021
Revised: June 29, 2022
Accepted: September 18, 2022
Published: October 13, 2022

REFERENCES

Alam, M.K., Alhhazmi, A., Decoteau, J.F., Luo, Y., and Geyer, C.R. (2016). RecA inhibitors potentiate antibiotic activity and block evolution of antibiotic resistance. Cell Chem. Biol. *23*, 381–391.

Appelbaum, P.C. (2012). 2012 and beyond: potential for the start of a second pre-antibiotic era? J. Antimicrob. Chemother. *67*, 2062–2068.

Baharoglu, Z., and Mazel, D. (2014). SOS, the formidable strategy of bacteria against aggressions. FEMS Microbiol. Rev. *38*, 1126–1145.

Beaber, J.W., Hochhut, B., and Waldor, M.K. (2004). SOS response promotes horizontal dissemination of antibiotic resistance genes. Nature *427*, 72–74.

Bellio, P., Di Pietro, L., Mancini, A., Piovano, M., Nicoletti, M., Brisdelli, F., Tondi, D., Cendron, L., Franceschini, N., Amicosante, G., et al. (2017). SOS response in bacteria: inhibitory activity of lichen secondary metabolites against Escherichia coli RecA protein. Phytomedicine *29*, 11–18.

Bellio, P., Mancini, A., Di Pietro, L., Cracchiolo, S., Franceschini, N., Reale, S., de Angelis, F., Perilli, M., Amicosante, G., Spyrakis, F., et al. (2020). Inhibition of the transcriptional repressor LexA: withstanding drug resistance by inhibiting the bacterial mechanisms of adaptation to antimicrobials. Life Sci. *241*, 117116.

Blázquez, J. (2003). Hypermutation as a factor contributing to the acquisition of antimicrobial resistance. Clin. Infect. Dis. *37*, 1201–1209.

Blázquez, J., Rodríguez-Beltrán, J., and Matic, I. (2018). Antibiotic-induced genetic variation: how it arises and how it can be prevented. Annu. Rev. Microbiol. *72*, 209–230.

Boshoff, H.I.M., Reed, M.B., Barry, C.E., and Mizrahi, V. (2003). DnaE2 polymerase contributes to in vivo survival and the emergence of drug resistance in Mycobacterium tuberculosis. Cell *113*, 183–193.

Butala, M., Klose, D., Hodnik, V., Rems, A., Podlesek, Z., Klare, J.P., Anderluh, G., Busby, S.J., Steinhoff, H.J., and Zgur-Bertok, D. (2011). Interconversion between bound and free conformations of Lexa orchestrates the bacterial SOS response. Nucleic Acids Res. *39*, 6546–6557.

Butala, M., Žgur-Bertok, D., and Busby, S.J.W. (2009). The bacterial LexA transcriptional repressor. Cell. Mol. Life Sci. *66*, 82–93.

Caveney, N.A., Pavlin, A., Caballero, G., Bahun, M., Hodnik, V., de Castro, L., Fornelos, N., Butala, M., and Strynadka, N.C.J. (2019). Structural insights into bacteriophage GIL01 gp7 inhibition of host LexA repressor. Structure *27*, 1094–1102.e4.

Chellappa, S.T., Maredia, R., Phipps, K., Haskins, W.E., and Weitao, T. (2013). Motility of Pseudomonas aeruginosa contributes to SOS-inducible biofilm formation. Res. Microbiol. *164*, 1019–1027.

Cirz, R.T., and Romesberg, F.E. (2007). Controlling mutation: intervening in evolution as a therapeutic strategy. Crit. Rev. Biochem. Mol. Biol. *42*, 341–354.

Cirz, R.T., Chin, J.K., Andes, D.R., De Crécy-Lagard, V., Craig, W.A., and Romesberg, F.E. (2005). Inhibition of mutation and combating the evolution of antibiotic resistance. PLoS Biol. *3*, 1024–1033.

Cirz, R.T., Jones, M.B., Gingles, N.A., Minogue, T.D., Jarrahi, B., Peterson, S.N., and Romesberg, F.E. (2007). Complete and SOS-mediated response of Staphylococcus aureus to the antibiotic ciprofloxacin. J. Bacteriol. *189*, 531–539.

Culyba, M.J., Kubiak, J.M., Mo, C.Y., Goulian, M., and Kohli, R.M. (2018). Non-equilibrium repressor binding kinetics link DNA damage dose to transcriptional timing within the SOS gene network. PLoS Genet *14*, e1007405.

Culyba, M.J., Mo, C.Y., and Kohli, R.M. (2015). Targets for combating the evolution of acquired antibiotic resistance. Biochemistry *54*, 3573–3582.

Danquah, W., Catherine, M.S., Rissiek, B., Pinto, C., Arnau, S.P., Amadi, M., Iacenda, D., Knop, J.H., Hammel, A., Bergmann, P., et al. (2016). Nanobodies that block gating of the P2X7 ion channel ameliorate inflammation. Sci. Transl. Med. *8*, 366ra162.

Dolinsky, T.J., Nielsen, J.E., McCammon, J.A., and Baker, N.A. (2004). PDB2PQR: an automated pipeline for the setup of Poisson-Boltzmann electrostatics calculations. Nucleic Acids Res. *32*, W665–W667.

Emsley, P., Lohkamp, B., Scott, W.G., and Cowtan, K. (2010). Features and development of Coot. Acta Crystallogr. Sect. D Biol. Crystallogr. *66*, 486–501.

Errasti-Murugarren, E., Fort, J., Bartoccioni, P., Díaz, L., Pardon, E., Carpena, X., Espino-Guarch, M., Zorzano, A., Ziegler, C., Steyaert, J., et al. (2019). L amino acid transporter structure and molecular bases for the asymmetry of substrate interaction. Nat. Commun. *10*, 1–12.

European Centre for Disease Prevention and Control (ECDC) (2009). Antimicrobial Resistance Surveillance in Europe: Annual Report of the European Antimicrobial Resistance Surveillance Network (EARS-Net).

Fernández De Henestrosa, A.R., Ogi, T., Aoyagi, S., Chafin, D., Hayes, J.J., Ohmori, H., and Woodgate, R. (2000). Identification of additional genes belonging to the LexA regulon in Escherichia coli. Mol. Microbiol. *35*, 1560–1572.

Fornelos, N., Butala, M., Hodnik, V., Anderluh, G., Bamford, J.K., and Salas, M. (2015). Bacteriophage GIL01 gp7 interacts with host LexA repressor to enhance DNA binding and inhibit RecA-mediated auto-cleavage. Nucleic Acids Res. *43*, 7315–7329.

Foti, J.J., Simmons, L.A., Beuning, P.J., and Walker, G.C. (2010). Signal transduction in the Escherichia coli SOS response. In Handbook of Cell Signaling (Elsevier), pp. 2127–2136.

Fumey, W., Koenigsdorf, J., Kunick, V., Menzel, S., Schütze, K., Unger, M., Schriewer, L., Haag, F., Adam, G., Oberle, A., et al. (2017). Nanobodies effectively modulate the enzymatic activity of CD38 and allow specific imaging of CD38+ tumors in mouse models in vivo. Sci. Rep. *7*, 1–13.

Giese, K.C., Michalowski, C.B., and Little, J.W. (2008). RecA-dependent cleavage of LexA dimers. J. Mol. Biol. *377*, 148–161.

Goormaghtigh, F., and Van Melderen, L. (2019). Single-cell imaging and characterization of Escherichia coli persister cells to ofloxacin in exponential cultures. Sci. Adv. *5*, eaav9462.

Harms, A., Maisonneuve, E., and Gerdes, K. (2016). Mechanisms of bacterial persistence during stress and antibiotic exposure. Science *354*.

Hostetler, Z.M., Cory, M.B., Jones, C.M., Petersson, E.J., and Kohli, R.M. (2020). The kinetic and molecular basis for the interaction of LexA and activated RecA revealed by a fluorescent amino acid probe. ACS Chem. Biol. *15*, 1127–1133.

Jolivet-Gougeon, A., and Bonnaure-Mallet, M. (2014). Biofilms as a mechanism of bacterial resistance. Drug Discov. Today Technol. *11*, 49–56.

Jurrus, E., Engel, D., Star, K., Monson, K., Brandi, J., Felberg, L.E., Brookes, D.H., Wilson, L., Chen, J., Liles, K., et al. (2018). Improvements to the APBS biomolecular solvation software suite. Protein Sci. *27*, 112–128.

Krissinel, E., and Henrick, K. (2007). Inference of macromolecular assemblies from crystalline state. J. Mol. Biol. *372*, 774–797.

Laskowski, R.A., Watson, J.D., and Thornton, J.M. (2005). ProFunc: a server for predicting protein function from 3D structure. Nucleic Acids Res. *33*, W89–W93.

Liebschner, D., Afonine, P.V., Baker, M.L., Bunkoczi, G., Chen, V.B., Croll, T.I., Hintze, B., Hung, L.W., Jain, S., McCoy, A.J., et al. (2019). Macromolecular structure determination using X-rays, neutrons and electrons: recent developments in Phenix. Acta Crystallogr. Sect. D Struct. Biol. *75*, 861–877.

Lu, T.K., and Collins, J.J. (2009). Engineered bacteriophage targeting gene networks as adjuvants for antibiotic therapy. Proc. Natl. Acad. Sci. USA *106*, 4629–4634.

Luo, Y., Pfuetzner, R.A., Mosimann, S., Paetzel, M., Frey, E.A., Cherney, M., Kim, B., Little, J.W., and Strynadka, N.C.J. (2001). Crystal structure of LexA: a conformational switch for regulation of self-cleavage. Cell *106*, 585–594.

Maslowska, K.H., Makiela-Dzbenska, K., and Fijalkowska, I.J. (2019). The SOS system: a complex and tightly regulated response to DNA damage. Environ. Mol. Mutagen. *60*, 368–384.

McCoy, A.J., Grosse-Kunstleve, R.W., Adams, P.D., Winn, M.D., Storoni, L.C., and Read, R.J. (2007). Phaser crystallographic software. J. Appl. Crystallogr. *40*, 658–674.

Miller, C., Thomsen, L.E., Gaggero, C., Mosseri, R., Ingmer, H., and Cohen, S.N. (2004). SOS response induction by β-lactams and bacterial defense against antibiotic lethality. Science *305*, 1629–1631.

Mo, C.Y., Birdwell, L.D., and Kohli, R.M. (2014). Specificity determinants for autoproteolysis of LexA, a key regulator of bacterial SOS mutagenesis. Biochemistry *53*, 3158–3168.

Mo, C.Y., Manning, S.A., Roggiani, M., Culyba, M.J., Samuels, A.N., Sniegowski, P.D., Goulian, M., and Kohli, R.M. (2016). Systematically altering bacterial SOS activity under stress reveals therapeutic strategies for potentiating antibiotics. mSphere *1*.

Mo, C.Y., Culyba, M.J., Selwood, T., Kubiak, J.M., Hostetler, Z.M., Jurewicz, A.J., Keller, P.M., Pope, A.J., Quinn, A., Schneck, J., et al. (2018). Inhibitors of LexA autoproteolysis and the bacterial SOS response discovered by an Academic-Industry Partnership. ACS Infect. Dis. *4*, 349–359.

Mok, W.W.K., and Brynildsen, M.P. (2018). Timing of DNA damage responses impacts persistence to fluoroquinolones. Proc. Natl. Acad. Sci. USA *115*, E6301–E6309.

Murshudov, G.N., Skubák, P., Lebedev, A.A., Pannu, N.S., Steiner, R.A., Nicholls, R.A., Winn, M.D., Long, F., and Vagin, A.A. (2011). REFMAC5 for the refinement of macromolecular crystal structures. Acta Crystallogr. Sect. D Biol. Crystallogr. *67*, 355–367.

Nautiyal, A., Patil, K.N., and Muniyappa, K. (2014). Suramin is a potent and selective inhibitor of Mycobacterium tuberculosis RecA protein and the SOS response: RecA as a potential target for antibacterial drug discovery. J. Antimicrob. Chemother. *69*, 1834–1843.

Nübel, U. (2016). Emergence and spread of antimicrobial resistance: recent insights from bacterial population genomics. Curr. Top. Microbiol. Immunol. *398*, 35–53.

Pardon, E., Laeremans, T., Triest, S., Rasmussen, S.G.F., Wohlkönig, A., Ruf, A., Muyldermans, S., Hol, W.G.J., Kobilka, B.K., and Steyaert, J. (2014). A general protocol for the generation of nanobodies for structural biology. Nat. Protoc. *9*, 674–693.

Pardon, E., Betti, C., Laeremans, T., Chevillard, F., Guillemyn, K., Kolb, P., Ballet, S., and Steyaert, J. (2018). Nanobody-enabled reverse pharmacology on G-protein-coupled receptors. Angew. Chemie - Int. Ed. *57*, 5292–5295.

Radman, M. (1975). SOS repair hypothesis: phenomenology of an inducible DNA repair which is accompanied by mutagenesis. In Molecular Mechanisms for Repair of DNA, P.C. Hanawalt and R.B. Setlow, eds. (Springer US), pp. 355–367.

Recacha, E., Machuca, J., Díaz-Díaz, S., García-Duque, A., Ramos-Guelfo, M., Docobo-Pérez, F., Blázquez, J., Pascual, A., and Rodríguez-Martínez, J.M. (2019). Suppression of the SOS response modifies spatiotemporal evolution, post-antibiotic effect, bacterial fitness and biofilm formation in quinolone-resistant Escherichia coli. J. Antimicrob. Chemother. *74*, 66–73.

Rice, L.B. (2008). Federal funding for the study of antimicrobial resistance in nosocomial pathogens: No ESKAPE. J. Infect. Dis. *197*, 1079–1081.

Rueden, C.T., Schindelin, J., Hiner, M.C., DeZonia, B.E., Walter, A.E., Arena, E.T., and Eliceiri, K.W. (2017). ImageJ2: ImageJ for the next generation of scientific image data. BMC Bioinf. *18*, 529.

Santajit, S., and Indrawattana, N. (2016). Mechanisms of antimicrobial resistance in ESKAPE pathogens. BioMed Res. Int. https://doi.org/10.1155/2016/2475067.

Selwood, T., Larsen, B.J., Mo, C.Y., Culyba, M.J., Hostetler, Z.M., Kohli, R.M., Reitz, A.B., and Baugh, S.D.P. (2018). Advancement of the 5-amino-1-(carbamoylmethyl)-1H- 1,2,3-triazole-4-carboxamide scaffold to disarm the bacterial SOS response. Front. Microbiol. *9*, 2961.

Short, J.M., Liu, Y., Chen, S., Soni, N., Madhusudhan, M.S., Shivji, M.K.K., and Venkitaraman, A.R. (2016). High-resolution structure of the presynaptic RAD51 filament on single-stranded DNA by electron cryo-microscopy. Nucleic Acids Res. *44*, 9017–9030.

Simmons, L.A., Foti, J.J., Cohen, S.E., and Walker, G.C. (2008). The SOS regulatory network. EcoSal Plus *3*, 5.4.3.

Singletary, L.A., Gibson, J.L., Tanner, E.J., McKenzie, G.J., Lee, P.L., Gonzalez, C., and Rosenberg, S.M. (2009). An SOS-regulated type 2 toxin-antitoxin system. J. Bacteriol. *191*, 7456–7465.

Slilaty, S.N., Rupley, J.A., and Little, J.W. (1986). Intramolecular cleavage of LexA and phage λ repressors: dependence of kinetics on repressor concentration, pH, temperature, and solvent. Biochemistry *25*, 6866–6875.

Stevenson, C.E.M., and Lowson, D.M. (2021). Analysis of protein–DNA interactions using surface plasmon resonance and a ReDCaT chip. Methods Mol. Biol. *2263*, 369–379.

Strugeon, E., Tilloy, V., Ploy, M.C., and Da Re, S. (2016). The stringent response promotes antibiotic resistance dissemination by regulating integron integrase expression in biofilms. mBio *7*.

Tiwari, V., Tiwari, M., and Biswas, D. (2018). Rationale and design of an inhibitor of RecA protein as an inhibitor of Acinetobacter baumannii. J. Antibiot. (Tokyo) *71*, 522–534.

Vascon, F., Gasparotto, M., Giacomello, M., Cendron, L., Bergantino, E., Filippini, F., and Righetto, I. (2020). Protein electrostatics: from computational and structural analysis to discovery of functional fingerprints and biotechnological design. Comput. Struct. Biotechnol. J. *18*, 1774–1789.

Walter, B.M., Rupnik, M., Hodnik, V., Anderluh, G., Dupuy, B., Paulič, N., Žgur-Bertok, D., and Butala, M. (2014). The LexA regulated genes of the Clostridium difficile. BMC Microbiol. *14*, 88.

Waterhouse, A., Bertoni, M., Bienert, S., Studer, G., Tauriello, G., Gumienny, R., Heer, F.T., De Beer, T.A.P., Rempfer, C., Bordoli, L., et al. (2018). SWISS-MODEL: Homology modelling of protein structures and complexes. Nucleic Acids Res. *46*, W296–W303.

Wigle, T.J., and Singleton, S.F. (2007). Directed molecular screening for RecA ATPase inhibitors. Bioorg. Med. Chem. Lett. *17*, 3249–3253.

Winn, M.D., Ballard, C.C., Cowtan, K.D., Dodson, E.J., Emsley, P., Evans, P.R., Keegan, R.M., Krissinel, E.B., Leslie, A.G.W., McCoy, A., et al. (2011). Overview of the CCP4 suite and current developments. Acta Crystallogr. Sect. D Biol. Crystallogr. *67*, 235–242.

Xing, X., and Bell, C.E. (2004). Crystal structures of Escherichia coli RecA in complex with MgADP and MnAMP-PNP. Biochemistry *43*, 16142–16152.

Xu, J., Zhao, L., Xu, Y., Zhao, W., Sung, P., and Wang, H.W. (2017). Cryo-EM structures of human RAD51 recombinase filaments during catalysis of DNA-strand exchange. Nat. Struct. Mol. Biol. *24*, 40–46.

Yakimov, A., Pobegalov, G., Bakhlanova, I., Khodorkovskii, M., Petukhov, M., and Baitin, D. (2017). Blocking the RecA activity and SOS-response in bacteria with a short α-helical peptide. Nucleic Acids Res. *45*, 9788–9796.

Yeeles, J.T.P., and Marians, K.J. (2013). Dynamics of leading-strand lesion skipping by the replisome. Mol. Cell *52*, 855–865.

Yu, X., Jacobs, S.A., West, S.C., Ogawa, T., and Egelman, E.H. (2001). Domain structure and dynamics in the helical filaments formed by RecA and Rad51 on DNA. Proc. Natl. Acad. Sci. USA *98*, 8419–8424.

Zhang, A.P.P., Pigli, Y.Z., and Rice, P.A. (2010). Structure of the LexA-DNA complex and implications for SOS box measurement. Nature *466*, 883–886.

STAR★METHODS

KEY RESOURCES TABLE

REAGENT or RESOURCE	SOURCE	IDENTIFIER
Antibodies		
His Tag mouse monoclonal antibody	Proteintech	Cat#66005-1-Ig
Amersham ECL Mouse IgG, HRP-linked whole Ab (from sheep)	Cytiva	Cat#NA931-100UL
Anti-LexA Antibody, rabbit polyclonal	Merck	Cat#06-719
Goat Anti-rabbit IgG secondary antibody, HRP-conjugated	Sino Biological	Cat#SSA004
Bacterial and virus strains		
Escherichia coli ATCC 25922	LGC/ATCC	N/A
Escherichia coli SMR6669 (*psulA::gfp*)	Singletary et al., 2009	N/A
Escherichia coli BL21(DE3)	New England Biolabs	N/A
Escherichia coli WK6	Pardon et al., 2014	N/A
Chemicals, peptides, and recombinant proteins		
FlAsH-EDT$_2$	Toronto Research Chemicals	Cat#F335200
ATPγS	Jena Bioscience	Cat#NU-406
Streptavidin-HRP	Thermo Fisher	Cat#21130
TMB Substrate Solution	Thermo Fisher	Cat#N301
SUMO Protease	Invitrogen	Cat#12588-018
TRIzol reagent	Thermo Fisher	Cat# 15596026
RQ1 RNase-Free DNAseI	Promega	Cat#M6101
SensiFAST SYBR® No-ROX mix	Bioline	Cat#BIO-98005
Pierce™ ECL Western Blotting Substrate	Thermo Fisher	Cat#32109
SYBR® Gold Nucleic Acid Gel Stain	Invitrogen	Cat#S11494
SYPRO™ Ruby Protein Gel Stain	Invitrogen	Cat#S12001
Fluoroshield™ with DAPI	Sigma-Aldrich	Cat# F6057
Streptavidin	Jackson Immuno Research	Cat#016-000-084
CaptureSelect Biotin anti-C-tag Conjugate	LifeTechnologies	Cat#7103252100
Streptavidin Alkaline Phosphatase	Promega	Cat#V5591
GERBU Adjuvant LQ 3000	GERBU Biotechnik	Cat#30000025
Critical commercial assays		
QuikChange™ II Site-Directed Mutagenesis Kit	Agilent Technologies	Cat#200518
FIREScript® RT cDNA synthesis KIT	Solis BioDyne	Cat#06-15-00050
Morpheus, LMB, PACT Premier and JCSG Plus crystallization kits	Molecular Dimensions	Cat#MD1-123, MD1-98, MD1-29, MD1-37
Deposited data		
Crystal structure of LexA-NbSOS1	This work	PDB 7ZRA
Crystal structure of LexA-NbSOS2	This work	PDB 7OCJ
Crystal structure of LexA-NbSOS3	This work	PDB 7B5G
Oligonucleotides		
SKBT25-18mer (5′-GCGTGTGTGGTGGTGTGC-3′)	Giese et al., 2008	N/A
SOSbox.fw (5′-GATGCCT GCGGATACTGT ATATATATACAGTATCAA TTCTGGCT-3′)	Zhang et al., 2010	N/A

(*Continued on next page*)

Continued

REAGENT or RESOURCE	SOURCE	IDENTIFIER
SOSbox.rv (5′-AGCCA GAATTGATACTGTAT ATATATACAGTATC CGCAGGCATC-3′)	Zhang et al., 2010	N/A
ReDCaT (5'-[BtnTEG]-GGC AGGAGGACGTAGGGT AGG-3′)	Stevenson and Lawson, 2021	N/A
ReDCaT-SOSbox.rv (5′-AGCCAGAATT GATACTGTATATA GGCATCCCTAC CCTACGTCC TCCTGC-3′)	This work	N/A
Primers used in molecular cloning and qPCR are listed in Table S1.	This work	N/A
Recombinant DNA		
pMESy4	Pardon et al., 2014	GenBank KF415192
pMESy4-NbSOS1 - 3	This work	N/A
pRham C-His Kan Vector	Lucigen	Cat#49012-2
pRham-NbSOS1 - 3	This work	N/A
pET28b-NHis-LexA	Bellio et al., 2020	N/A
pET28b-NHis-LexA-S119A	This work	N/A
pET28b-NHis-LexA-G85D	This work	N/A
pET28b-NHis-RecA	Bellio et al., 2017	N/A
pColiExpress™ I	Canvax Biotech	Cat#BE001
pColiExpressI-LexACTD	This work	N/A
pColiExpressI-LexACTD-S119A	This work	N/A
pColiExpressI-LexACTD-G85D	This work	N/A
Champion™ pET SUMO vector	Invitrogen	Cat#K30001
pET-NHis-SUMO-4Cys-LexA CTD	This work	N/A
pET-NHis-SUMO-4Cys-LexA CTD S119A	This work	N/A
Software and algorithms		
Fiji	Rueden et al., 2017	https://imagej.net/software/fiji/
GraphPad Prism v7.00	GraphPad	https://www.graphpad.com/
FlowJo 10.4	BD Biosciences	https://www.flowjo.com/
Matlab R2017b	MathWorks	https://www.mathworks.com
CCP4i2	Winn et al., 2011	https://www.ccp4.ac.uk/
Phenix	Liebschner et al., 2019	https://phenix-online.org/
Biacore T100 Evaluation Software	Cytiva	https://www.cytivalifesciences.com/
StepOne Software	Applied Biosystems	https://www.thermofisher.com/it/en/home/technical-resources/software-downloads/StepOne-and-StepOnePlus-Real-Time-PCR-System.html
PyMol v2.0	Schrödinger LLC	https://pymol.org/2/
UCSF Chimera	RBVI, University of California	https://www.cgl.ucsf.edu/chimera/
Other		
HisTrap HP His tag protein purification columns (1 mL and 5 mL)	Ge Healthcare	Cat#17524801 Cat#29051021
Series S Sensor Chip CM5	Cytiva	Cat#BR100530

RESOURCE AVAILABILITY

Lead contact

Further information and requests for resources and reagents should be directed to and will be fulfilled by the lead contact, Laura Cendron (laura.cendron@unipd.it).

Materials availability

All constructs used in this study are available upon reasonable request from the lead contact. All constructs were sequence-verified via Sanger sequencing.

Data and code availability

- The data generated in this study are available upon reasonable request from the lead contact. X-ray structures of LexA-NbSOSs complexes have been deposited at PDB and are publicly available as of the date of publication. Accession numbers are listed in the key resources table.
- This paper does not report original code.
- Any additional information required to reanalyze the data reported in this paper is available from the lead contact upon request.

EXPERIMENTAL MODEL AND SUBJECT DETAILS

Animals

An adult male llama was immunized with the RecA*/LexA complex as described below. All vaccination procedures were executed in accordance with the applicable animal welfare legislation, and they were approved by the local ethics committee.

Microbe strains

E. coli BL21(DE3) and WK6 strains were used for protein expression and cultured in LB or Terrific Broth medium supplemented with the opportune antibiotic, as further detailed in the following paragraphs. *E. coli* ATCC 25922 and SMR6669 were used for testing NbSOSs activity *in vivo* and cultured at 37°C in LB medium.

METHOD DETAILS

Recombinant genes cloning and mutagenesis

Plasmid pET28b-NHis-LexA, harboring the full-length *Escherichia coli lexA* gene was exploited to overexpress N-terminal His-tagged LexA as previously reported (Bellio et al., 2020).

Uncleavable mutants G85D and S119A of *E. coli* LexA were obtained by site-directed mutagenesis of pET28b-NHis-LexA plasmid using the QuikChange™ II Site-Directed Mutagenesis Kit (Agilent Technologies) according to the kit protocol, using primers couples reported in Table S1. Plasmids used for the expression of LexA C-terminal domain (CTD; residues 75-202) of uncleavable LexA mutants G85D and S119A were obtained sub-cloning the CTD coding sequences from pET28b-NHis-LexA G85D and pET28b-NHis-LexA S119A respectively, into pColiExpress™ I plasmid (coding for N-terminal 6xHis-tag; Canvax Biotech) according to manufacturer's instructions, using primers LexA_CTD.fw and LexA_CTD.rv reported in Table S1. These plasmids encode ampicillin resistance selectable marker. The LexA construct exploited for FP measurements was designed and cloned as already reported (Mo et al., 2018), with slight variations. Briefly, the coding sequence of LexA CTD was amplified by PCR from pET28b-NHis-LexA plasmid with primers (LexA_FlAsH.fw/rv; Table S1) introducing a sequence coding for an N-terminal tetracysteine tag (-CCPGCC-). The obtained PCR product was cloned into Champion™ pET SUMO vector (Invitrogen) via TA cloning, following manufacturer's instructions. The final construct (pET-NHis-SUMO-4Cys-LexA CTD) allows the production of a 6xHis-SUMO-CCPGCC tagged LexA CTD. The plasmid encodes kanamycin resistance selectable marker. The inactivating mutation S119A was introduced in pET-NHis-SUMO-4Cys-LexA CTD by the QuikChange™ II Site-Directed Mutagenesis Kit (Agilent Technologies) according to the kit protocol, using primers reported in Table S1.

Plasmid pET28b-N-His-RecA, harboring the full-length *E. coli recA* gene in frame with 6xHis-tag at the N-terminus, was exploited to overexpress RecA recombinase as previously described (Bellio et al., 2017). Plasmids encoding NbSOS1, NbSOS2 and NbSOS3, exploited for Nbs expression and purification, derive from pMESy4 vector, which allows the periplasmic secretion, IMAC purification and immune-detection of the nanobodies thanks to an N-terminal PelB leader sequence and C-terminal 6xHis-Tag and CaptureSelect C-tag, respectively. All these three plasmids belong to a library developed in collaboration with the VIB-VUB Center for Structural Biology (Steyaert lab) and they have all been obtained according to the protocol described by Pardon and colleagues (Pardon et al., 2014). To perform *in vivo* analysis of SOS response suppression upon NbSOSs expression, the ORFs of NbSOS1, NbSOS2 and NbSOS3 were sub-cloned into pRham C-His Kan Vector (Lucigen) according to manufacturer's protocol, using the primers listed in Table S1. A control empty pRham vector was obtained too, screening for closed plasmids and verifying the absence of any insert. The sequence of all the reported constructs was verified by Sanger DNA sequencing (performed by BMR Genomics, Padova, Italy). pMESy4 and pRham-derived vectors encode ampicillin and kanamycin resistance selectable gene markers, respectively.

Protein expression and purification

LexA variants (LexA, LexA^{G85D}, LexA^{S119}, LexA$^{75-202(G85D)}$)

Full-length and CTD LexA, either wild type or bearing mutations G85D or S119A, were all produced and purified as described below. *E. coli* BL21(DE3) cells (New England Biolabs) were transformed with the appropriate expression vector and grown in LB medium supplemented with antibiotic at 37°C. Protein overexpression was induced with 1 mM Isopropyl-β-D-1-thiogalactopyranoside (IPTG) once the OD_{600} of the culture reached 0.5, and cultures were kept at 37°C for additionally 3 h. Bacterial cells were harvested by centrifugation and resuspended in LexA lysis buffer (20 mM Tris-HCl pH 7.5, 150 mM NaCl, 10% glycerol, 25 mM imidazole), supplemented with 1X Roche protein inhibitors cocktail and processed by French press. His-tagged LexA was purified from the soluble fraction of the lysate by IMAC using a HisTrap HP 1 mL column (GE Healthcare). After extensive column washing with LexA lysis buffer, His tagged LexA was eluted with Buffer B (20 mM Tris-HCl pH 7.5, 150 mM NaCl, 10% glycerol, 0.5 M imidazole). A final step of purification was performed by size exclusion chromatography on Superose 12 10/300 GL column (GE Healthcare) in final buffer (30 mM HEPES pH 7.1, 150 mM NaCl, 10% glycerol), and most pure fractions containing LexA dimers were concentrated and stored in small aliquots at −80°C or directly used for experimental purposes.

FlAsH-LexA$^{75-202}$ and FlAsH-LexA$^{75-202(S119A)}$

LexA autoproteolysis inhibition and RecA*-LexA binding assays relying on fluorescence polarization were performed using FlAsH-LexA$^{75-202}$ and its S119A uncleavable mutant (the latter is needed to isolate the binding event from the autoproteolysis step), which were obtained by expression, purification and processing of the fusion proteins encoded by pET-NHis-SUMO-4Cys-LexA CTD and pET-NHis-SUMO-4Cys-LexA CTD S119A, using the following method.

N-His-SUMO-4Cys-LexA CTD was expressed in *E. coli* BL21(DE3) cells and IMAC-purified following the same protocol reported for LexA variants but carrying out protein overexpression at room temperature overnight following IPTG-mediated induction and adding 0.1 mM DTT to the lysis buffer. IMAC fractions containing the N-His-SUMO-4Cys-LexA CTD fusion protein were diluted in 20 mM Tris-HCl, pH 7.5, 150 mM NaCl, 10% glycerol, 0.1 mM DTT until imidazole concentration dropped below 150 mM and supplemented with 1 mM DTT, 1 mM EDTA, 0.1% v/v NP40 and SUMO protease. N-His-SUMO tag cleavage reaction by SUMO protease was carried out for 2 h at 25°C. Next, the fluorescent labeling reaction was performed with the addition of a 2-fold molar excess of FlAsH-EDT_2 (Toronto Research Chemicals) to the mixture and carried out overnight at 4°C protected from light. Following cleavage and labeling, the protein mixture was buffer exchanged to final buffer (20 mM Tris-HCl pH 7.5, 150 mM NaCl, 10% glycerol) to remove excess of NP40, unbound FlAsH-EDT_2, DTT and EDTA. FlAsH-LexA$^{75-202}$ was then isolated from uncleaved N-His-SUMO-4Cys-LexA CTD, N-His-SUMO fragments and His-tagged SUMO protease by IMAC (HisTrap HP 1 mL column, GE Healthcare), recovering the flow-through. FlAsH-LexA$^{75-202}$ fractions were concentrated and stored in small aliquots protected from light at −80°C for fluorescence polarization assays.

RecA

Overexpression of His-tagged *E. coli* RecA was performed growing *E. coli* BL21(DE3) cells (New England Biolabs) bearing pET28b-N-His-RecA plasmid in LB medium (with 30 μg/mL kanamycin) at 37°C. Large scale expression was induced at 0.7 OD_{600} with 1 mM IPTG and carried out for 4 h at 37°C. Cell pellet was recovered by centrifugation, resuspended in lysis buffer (10 mM HEPES pH 8.0, 300 mM NaCl, 10% glycerol and 20 mM imidazole), supplemented with protease inhibitors cocktail (Roche) and lysed by French press. N-His-RecA was purified from lysate soluble fraction by IMAC (HisTrap HP 5 mL column, GE Healthcare) and eluted in Buffer B (10 mM HEPES pH 8.0, 300 mM NaCl, 10% v/v Glycerol, 0.5 M Imidazole). Fractions containing the desired protein, as evaluated by SDS-PAGE, were buffer exchanged with PD10 desalting columns (GE Healthcare) in RecA buffer (10 mM HEPES pH 7.0, 300 mM NaCl, 10% glycerol, 1 mM DTT and 1 mM $MgCl_2$). N-terminal His tag removal was performed by Thrombin digestion of the purified protein. Cleaved RecA was isolated and further purified by size exclusion chromatography (Superdex 200 Hiload 16/60 column, GE Healthcare) in RecA buffer, and most pure fractions were concentrated and stored in small aliquots at −80°C for all the different experimental purposes.

NbSOSs

Production and purification of the Nanobodies was carried out as described by Pardon and colleagues (Pardon et al., 2014). Briefly, Nanobodies overexpression was carried out in *E. coli* WK6 transformed with the above-mentioned pMESy4-NbSOS plasmids and cultured at 37°C in Terrific Broth supplemented with 100 μg/mL ampicillin, 0.1% glucose and 1 mM $MgCl_2$, until OD_{600} reached 0.7. Nanobodies expression was then induced by adding 1 mM IPTG, and the culture was grown overnight at 28°C. Following bacterial cell harvesting by centrifugation, the pellet was resuspended in ice-cold TES buffer (0.2 M Tris pH 8.0, 0.5 mM EDTA and 0.5 M sucrose) and incubated for 1 h on ice with shaking. Periplasmic extract was then obtained by adding two volumes of TES/4 buffer (25% v/v TES in ddH_2O) and incubating the suspension on ice for 45 min with shaking. His-tagged Nanobodies were purified from soluble periplasmic extract by IMAC (HisTrap HP 1 mL column, GE Healthcare), washing extensively the column with 50 mM Sodium Phosphate pH 7.0, 1 M NaCl, and then eluting the desired proteins with 50 mM Sodium Phosphate pH 7.0, 150 mM NaCl and 0.5 M imidazole. Most pure fractions containing Nanobodies, as assessed by SDS-PAGE, were pooled together and buffer exchanged in final buffer (30 mM HEPES pH 7.1, 150 mM NaCl, 10% glycerol), and directly used for experimental purposes or stored in small aliquots at −80°C.

RecA activation

Biologically-active RecA/ssDNA oligomers used throughout the work were produced incubating RecA on ice at 4°C overnight in presence of SKBT25-18mer ssDNA (5′-GCGTGTGTGGTGGTGTGC-3′) at 1:3.5 molar ratio (ssDNA:RecA) and a 10-fold molar excess

of ATPγS. The resulting activated RecA (RecA*) kept its LexA autoproteolysis activation ability for a couple of days if stored at 4°C or for several weeks if stored at −20°C.

Antigen preparation, llama immunization and nanobodies discovery

The antigen exploited for llama immunization to obtain the Nanobodies library was a mildly crosslinked complex of RecA* and a mixture of wt LexA and $LexA^{S119A}$. Briefly, both LexA and $LexA^{S119A}$ (1:10) were incubated with RecA* (0.3:3:1 molar ratio LexA: $LexA^{S119A}$: RecA*) in 10 mM HEPES pH 7.0, 300 mM NaCl, 10% v/v Glycerol, 1 mM DTT, 1 mM $MgCl_2$, for 5 min at room temperature. Then cross-linker disuccinimidyl suberate (DSS) was added at 0.3 mM final concentration and incubated in the mixture for 30 min at room temperature. Cross-linking reaction was stopped by addition of 10 mM Tris pH 7.5. The obtained samples were then divided into aliquots and stored at −80°C for immunization and discovery purposes. Coomassie-stained SDS-PAGE gels of the cross-linked samples revealed the expected heterogeneity of the sample, showing the presence of the single components as well as LexA dimers, RecA* and LexA-RecA* complexes (Figure S1). A single llama was used for immunization, applying weekly injections of the antigen in presence of GERBU adjuvant LQ 3000 (GERBU Biotechnik), over a period of six weeks. Four days after the last injection, blood was collected. All animal vaccinations were performed in strict agreement with good practices and the European Union animal welfare legislation. Then, construction of immune libraries and Nb selection via phage display were accomplished using previously reported protocols (Pardon et al., 2014).

Briefly, starting from the blood sample collected after llama immunization, the variable domains of the heavy-chain-only antibody repertoire were amplified and cloned in a pMESy4 phage display vector, which introduces a 6xHis-tag and CaptureSelect™ C-tag at the Nb C-terminal. The resulting Nb library was displayed on the surface of filamentous phages after rescue with the VCSM13 helper phage. Selection of antigen-specific recombinant phages was performed using four complementary panning approaches: (i) LexA-RecA* (2 μg) was solid phase-coated on polystyrene plates by unspecific adsorption in coating buffer ($NaHCO_3$ pH 8.2, 1 mM DTT) and selections were done in 10 mM HEPES pH 7.0, 300 mM NaCl, 1 mM $MgCl_2$, 1 mM DTT; (ii) $LexA^{S119A}$-RecA* (0,02 μg) was coated on polystyrene plates in coating buffer ($NaHCO_3$ pH 8.2, 1 mM DTT) and selections were done in 10 mM HEPES pH 7.0, 300 mM NaCl, 1 mM $MgCl_2$, 1 mM DTT; (iii) biotinylated $LexA^{S119A}$ was trapped on neutravidin-agarose beads in 30 mM HEPES pH 7.1, 150 mM NaCl and selections were done using the same buffer; (iv) biotinylated $LexA^{75\text{-}202\ (G85D)}$ was trapped on neutravidin-agarose beads in 30 mM HEPES pH 7.1, 150 mM NaCl and selections were done in the same buffer.

ELISA screening of isolated phages was performed in the same buffer and against the same antigen used for phage selection ($LexA^{S119A}$-RecA* was solid-phase immobilized on ELISA plates by direct unspecific adsorption while biotinylated $LexA^{S119A}$ and $LexA^{75\text{-}202\ (G85D)}$ were captured on neutravidin-coated wells). Nanobodies were detected by CaptureSelect™ Biotin anti-C-tag Conjugate, premixed with Streptavidin-Alkaline Phosphatase and the chromogenic substrate 4-Nitrophenyl phosphate disodium salt hexahydrate (2 mg/ml). All the positive clones were sequence analyzed.

Fluorescence polarization assays

Fluorescence Polarization (FP) was exploited in this work to study several steps of the SOS response activation and its nanobody-mediated inhibition: (i) binding of NbSOSs to LexA, (ii) LexA autocleavage and (iii) RecA*-LexA binding event. All FP experiments were performed in Nunc 384 shallow well black plates (Thermo Scientific) using a final volume of 20 μL/well and FP was measured by a PerkinElmer EnVision Multimode Plate Reader at 37°C. All the proteins used in these assays were diluted into FP buffer (30 mM HEPES pH 7.1, 150 mM NaCl).

FlAsH-$LexA^{75\text{-}202}$ and RecA* were used at a final concentration of 1 μM (1:1 M ratio), while Nanobodies were used at 2 μM final concentration in the initial screening for possible LexA inhibitors and in the range 0.01-100 μM for dose-response experiments. LexA cleavage by alkaline pH was induced by adding 6 μL of 100 mM CAPS pH 10.4, 200 mM NaCl, taking the reaction mixture to pH 9. All samples were produced in triplicates. The time course of the experiments involved a first 5-min measurement of FlAsH-$LexA^{75\text{-}202}$ basal FP signal, followed by Nanobodies (or FP buffer in control samples) manual injection and FP signal recording for 15 min. RecA* (or alkaline buffer) was lastly added and FP was read for 1 h.

In LexA autocleavage inhibition assay analysis, samples containing only FlAsH-$LexA^{75\text{-}202}$ were considered as negative controls (100% cleavage inhibition) while samples devoid of NbSOSs were considered as positive controls (0% cleavage inhibition). LexA percent cleavage inhibition in samples containing NbSOSs was estimated accordingly from FP values at 1 h incubation in the presence of RecA*, after subtraction of FP at the end of the 15 min incubation prior to RecA* addition (to take into account the FP signal contribution due to NbSOSs binding to FlAsH-$LexA^{75\text{-}202}$). IC_{50} values for each NbSOS were obtained plotting percent cleavage inhibition as a function of nanobody concentration and then fitting the data points with the "absolute IC_{50}" model in GraphPad Prism version 7.00.

In binding experiments analysis, FlAsH-$LexA^{75\text{-}202}$ was used at 100 nM concentration and instrument parameters optimized accordingly. No RecA* or alkaline buffer was added in this case. FP of samples devoid of NbSOSs was used as reference value (LexA fraction bound to Nb = 0), while FP of samples containing 100 μM of each NbSOS was considered as completely nanobody-bound LexA (LexA fraction bound to Nb = 1). FP values of the other samples were scaled accordingly and K_D values for each NbSOS were calculated plotting the obtained values of LexA fraction bound to NbSOS as a function of Nb concentration. Resulting data were fitted with a one-site binding (saturation) model using GraphPad Prism version 7.00.

To assess the ability of selected NbSOSs to interfere with RecA*-LexA binding, 200 nM FlAsH- $LexA^{75\text{-}202\ (S119A)}$ was incubated with different concentrations of RecA* (0.01–10 μM) and 10 μM putative competitors (except for control reactions), either being

NbSOSs or unlabeled LexA^{S119A} to validate the robustness of the assay (Hostetler et al., 2020). Mixtures were produced in triplicate and incubated 1h at 37°C before reading the FP signal. The contribution of NbSOSs binding to FlAsH-LexA$^{75-202\ (S119A)}$ FP signal was screened by subtracting the FP value of RecA*-devoid samples to all the samples treated with the same putative competitor. Then, subtracted FP values were normalized on control series to obtain the RecA*-LexA percent binding (0 μM RecA*, 0% binding; 10 μM RecA*, 100% binding). RecA*-LexA percent binding at different RecA* concentration in the presence of putative competitors was compared to control reactions by unpaired t-tests.

SDS-PAGE LexA autocleavage assay

Nanobodies inhibition of LexA autocleavage induced by RecA* was evaluated by SDS-PAGE in conditions as similar as possible to the ones of FP assay (protein concentrations, sample volume, buffer composition, temperature and incubation time), but exploiting full-length LexA instead of FlAsH-LexA$^{75-202}$. Negative control samples (containing just 1 μM LexA in FP buffer) and positive control samples (1 μM LexA and 1 μM RecA*) were always included.

After 15 min incubation of LexA with NbSOSs and 1 h incubation in the presence of RecA*, LexA autoproteolysis reaction was stopped resuspending samples in Laemmli sample buffer and boiling them 10 min at 100°C. Samples where then subjected to SDS-PAGE and Coomassie staining.

Quantification of the uncleaved fraction of full-length LexA was performed by densitometry using Fiji software (Rueden et al., 2017). Percent cleavage inhibition data as function of Nanobodies concentration were treated and fitted exactly as described above for Fluorescence Polarization LexA cleavage assays.

Surface Plasmon Resonance

Nanobodies affinity for LexA and their ability to bind operator-bound LexA were assessed by Surface Plasmon Resonance exploiting a BIAcore™ T100 system (GE Healthcare).

To estimate NbSOSs-LexA K_D, full-length LexA^{S119A} protein was opportunely diluted in a 10 mM sodium acetate buffer at pH 5.0 and covalently immobilized on a Series S CM5 sensor chip (carboxymethylated dextran surface; Cytiva) by amine-coupling chemistry to a final density of 575 resonance units. A flow cell with no immobilized protein was used as a control. Binding analysis was carried out in HBSN (10 mM HEPES, pH 7.4, 150 mM NaCl) as running buffer, applying a flow rate of 20 μL/min.

Kinetic experiments were performed by challenging chip immobilized LexA^{S119A} with nine different dilutions of the analytes (NbSOS1, NbSOS2 and NbSOS3), one of which was duplicated. A contact time of 240 s was followed by a 400 s dissociation phase.

After each nanobody injection, the chip surface was regenerated by an injection of 10 mM Glycine, pH 1.5 for 5 s at a flow rate of 30 μL/min; this treatment restored the baseline to the initial resonance unit value. Kinetic experiments were preceded by three start-up cycles (injecting only running buffer) and included a zero control (running buffer).

The response of the control flow cell was subtracted to each sensorgram (time course of the surface plasmon resonance signal) and the different sensorgrams were normalized to baseline. Steady state affinity analysis of the obtained sensorgrams was performed using the Biacore T100 Evaluation Software. Data were fitted in GraphPad Prism v7.00 using a specific binding model, with Hill slope. Two independent experiments were performed.

For studying NbSOSs binding to SOS box DNA-bound LexA, SPR experiments were carried out in HBSN supplemented by 0.5 mM $MgCl_2$. Streptavidin (Jackson Immuno Research) was immobilized on a series S CM5 sensor chip (Cytiva) by amine coupling to a final density of 700 RU, then 5′-biotinylated ReDCaT oligonucleotide was bound (100 RU) to the streptavidin-coated chip (Stevenson and Lawson, 2021). ReDCaT-SOS-box dsDNA was prepared by mixing equimolar amounts of ReDCaT-SOSbox.rv and SOSbox.fw oligonucleotides, heating the mixture at 95°C for 10 min and then allowing it to slowly cool to room temperature. 1 μM ReDCaT-SOS-box dsDNA was injected over the test flow cell at a flow rate of 10 μL/min until reaching a 230 RU increase. To evaluate the affinity of LexA^{S119A} for chip-immobilized SOS-box dsDNA, a single cycle experiment was performed by injecting 5 dilutions of LexA^{S119A} (12.5–200 nM) at a flow rate of 10 μL/min.

Conversely, to assess the binding of NbSOSs to operator-bound LexA, manual run experiments were carried out at a flow rate of 10 μL/min by injecting first 100 nM LexA^{S119A} for 240 s (reaching a 50-75 RU maximal signal compared to the reference flow cell), letting it dissociate for 600 s and then injecting two pulses of NbSOSs (120 s, 10 μL/min, 300 s dissociation) at increasing concentration (0.1 and 2 μM). LexA and NbSOSs were removed from chip by 3 regeneration steps with 0.5 M NaCl at 30 μL/min. To account for any unspecific binding event, control experiments were performed injecting 2 μM NbSOSs over chip-immobilized SOS-box DNA.

Gene expression analysis by Real-time quantitative PCR (RT-qPCR)

Escherichia coli ATCC 25922 strain was used for gene expression profiling. Bacteria were transformed with either empty pRham C-His vector (pRham∅; Lucigen) or pRham vectors bearing NbSOSs coding sequences (pRham-NbSOS1, pRham-NbSOS2 and pRham-NbSOS3) and grown in LB medium supplemented with 30 mg/L kanamycin. Nanobodies expression was induced with 0.1% w/v L-Rhamnose at 0.5 OD_{600} for 1 h at 37°C. The same amount of L-Rhamnose was added to cultures of bacteria transformed with empty vector to keep growing conditions as similar as possible. In cultures subjected to antibiotic stress, SOS response was induced with 0.8 mg/L Ciprofloxacin, while control cultures were left without Ciprofloxacin. All the cultures were grown for additional 3 h at 37°C and finally harvested for RNA extraction (or western blotting to check Nanobodies expression). Total RNA was extracted from 2 mL of pelleted cultures with TRIzol reagent (Thermo Fisher Scientific). RNA samples were treated with DNaseI (Promega) to eliminate possible genomic DNA contaminations and stored at −80°C until use. Total RNA was used for cDNA synthesis with random

primers (Solis BioDyne) and FIREScript Reverse Transcriptase (Solis BioDyne) according to the manufacturer's protocol. Real-time PCR was performed using SYBR Green Master mix (Bioline) and primers listed in Table S1. Technical and biological replicates were carried out for all qPCR reactions. An endogenous control (*gapA*) was used to normalize expression. RT-qPCR was analyzed exploiting ΔΔCt relative quantification of the StepOne™ Software (Applied Biosystems).

Western blotting

The effect of NbSOSs on full-length LexA stability in *E. coli* treated with SOS inductors was checked by western blot analysis. *E. coli* ATCC 25922 transformed with either pRhamØ, pRham-NbSOS1, pRham-NbSOS2 or pRham-NbSOS3 were grown at 37°C in LB medium with 50 μg/mL kanamycin to OD 0.5, before inducing nanobody expression by adding 0.2% w/v L-Rhamnose. After 1 h incubation, cultures were supplemented by 0.8 μg/mL ciprofloxacin to induce DNA damage and SOS response. Samples normalized on cultures OD were collected at different time-points after ciprofloxacin treatment (0, 1, 3 and 5 h) and the cell pellet was resuspended in Laemmli sample buffer and boiled at 100°C for SDS-PAGE analysis (4-20% polyacrylamide gel) and western blot transfer on a nitrocellulose membrane. The membrane was saturated with 5% w/v milk in TBST and LexA was detected using anti-LexA primary polyclonal antibody (Merck; 0.1 μg/mL in TBST, 5% milk, overnight incubation at 4°C), anti-rabbit-HRP secondary antibody (Sino Biological; 0.3 μg/mL in TBST, 2.5% milk, 2h at room temperature) and ECL chemiluminescence development (Thermo Fisher).

Western blotting analysis was employed also to check the expression level of NbSOSs in bacterial cultures subjected to SOS genes suppression profiling. Briefly, culture samples from different time points of the above-mentioned experiments were treated with Laemmli sample buffer and boiled for 10 min at 100°C. The same number of cells from the different cultures was sampled according to OD_{600}. Samples were loaded on SDS-PAGE (NuPAGE 4 - 12%, Bis-Tris, Thermo Fisher Scientific), blotted on nitrocellulose and the membrane saturated with 5% BSA. His-tagged NbSOSs expression was detected using primary anti-His tag antibody (1:3000 dilution, Proteintech) and secondary anti-mouse HRP conjugated antibody (1:2000 dilution, Cytiva), and revealed with ECL substrate (Thermo Fisher) and quantified by densitometry using Fiji software (Rueden et al., 2017).

Electrophoretic Mobility Shift Assay

Electrophoretic Mobility Shift Assay (EMSA) was used to confirm that NbSOSs could bind to SOS-box DNA-bound LexA. The SOS box was obtained from the annealing of complementary oligonucleotides (SOSbox.fw and SOSbox.rv; Sigma Aldrich) designed based on work from Zhang et al. (2010) and reported in Table S1. The oligonucleotides were diluted in equimolar concentration in annealing buffer (10 mM Tris-HCl pH 7.5, 50 mM NaCl, 1 mM EDTA), incubated at 95°C for 5 min and left cooling down at room temperature. Electrophoretic mobility shift assay was performed incubating 100 nM SOS box with $LexA^{S119A}$ (8 μM) at 25°C for 20 min in EMSA binding buffer (10 mM Tris-HCl pH 7.4, 150 mM KCl, 0.1 mM DTT, 0.1 mM EDTA). Different concentrations (8, 24, 48 μM) of each nanobody (NbSOS1, NbSOS2 and NbSOS3) was incubated with $LexA^{S119A}$-SOS box complex for 20 min at 25°C. The samples were run on native gel (NativePage 3-12%, Invitrogen). SOS box dsDNA and $LexA^{S119A}$-SOS box complexes were loaded separately as reference. The possible interaction of each Nanobody with the DNA fragment was verified by incubating NbSOSs (8 μM) with dsDNA. The DNA bands were detected by SYBR Gold (Invitrogen) while the proteins were detected with SYPRO Ruby (Invitrogen). The images were merged with the use of Fiji software (Rueden et al., 2017).

Crystallization, data collection, structure determination and analysis

All LexA – NbSOS complexes (1:1 molar ratio) were concentrated to 20 mg/mL and submitted to wide crystallization trials in multiple conditions (Morpheus, LMB, PACT Premier and JCSG Plus crystallization kits, Molecular Dimensions) exploiting an Orix8 Crystallization Robot (Douglas Instruments) in an isothermal vapor diffusion crystallization setup (0.8 μL total volume drops, 1:1 protein-precipitant ratio, 293 K). Best diffracting crystals of LexA – NbSOS1 were obtained with a precipitation buffer including 0.2 M calcium chloride, 0.1 M HEPES pH 7, 20% w/v PEG 6000, and optimized by microseeding. LexA – NbSOS2 complex gave the best crystals when precipitated with 0.1 M sodium citrate pH 5.5, 20% w/v PEG 3000, and optimized by microseeding. For LexA – NbSOS3 complex, best diffracting crystals were obtained with 0.15 M sodium chloride, 0.05 M HEPES pH 6.8, 24% w/v PEG3350 as precipitant buffer and optimized by microseeding.

In all cases, crystals were cryo-protected with 20% v/v ethylene glycol, added to the precipitant solution, and flash frozen in liquid nitrogen. Diffraction data were collected at the Swiss Light Source (SLS) at the Paul Scherrer Institut in Villigen (Switzerland), at the Diamond Light Source at the Harwell Science and Innovation Campus in Oxfordshire (UK) and at the ESRF Synchrotron Radiation Facility (Grenoble, France). Statistics and further details of the diffraction datasets are reported in Table S3. All the structures were solved through advanced molecular replacement by Phaser software (McCoy et al., 2007) using CCP4 (Winn et al., 2011) and Phenix (Liebschner et al., 2019) interfaces. Multi component phasing methods were explored in order to solve the phase problem, using LexA protein model (PDB 1JHF) and an *in silico* model of each NbSOS generated by SwissModel (Waterhouse et al., 2018). Refinement of the obtained models was carried out by Refmac5 (Murshudov et al., 2011), Phenix.refine (Liebschner et al., 2019) and manual adjustment by the graphic software Coot (Emsley et al., 2010). Completion of the models was achieved by water molecules fitting. PyMol molecular graphics software (Schrödinger LLC) was used to generate illustrations. LexA – NbSOS interface analysis for each one of the three LexA – NbSOS structures was carried out by PISA, Pro-Func and LigPLot web services at the European Bioinformatics Institute (http://www.ebi.ac.uk/pdbe/prot_int/pistart.html, http://www.ebi.ac.uk/thornton-srv/databases/ProFunc/, https://www.ebi.ac.uk/thornton-srv/software/LIGPLOT/) (Krissinel and Henrick, 2007; Laskowski et al., 2005).

Given the notable relevance of electrostatics in protein-protein interactions (Vascon et al., 2020), the structures of NbSOS1, NbSOS2, NbSOS3, the interacting LexA CTD dimers and a model of full-length LexA (built joining NTD from PDB 3JSO and CTD from PDB 7OCJ by a linker modeled with Modeller in UCSF Chimera) were submitted to the tools PDB2PQR (Dolinsky et al., 2004) and APBS (Jurrus et al., 2018) to analyze surface electrostatic potential (to simulate *E. coli* cytoplasm conditions, residues pKa calculation was performed by PROPKA at pH 7.5 while Poisson-Boltzmann electrostatics were computed at 0.2 M NaCl). Electrostatic potential maps were visualized by UCSF Chimera.

Fluorescent analysis of the SOS response induction

E. coli SMR6669 is an MG1655 derivative strain that carries a transcriptional fusion between the *sulA* promoter and the *gfp* gene (*psulA::gfp*, integrated at the chromosomal *att*λ site), which was previously shown to be a sensitive and specific reporter for the induction of the SOS response in live cells (Goormaghtigh and Van Melderen, 2019; Singletary et al., 2009). This strain was transformed with either pRham∅ (control) or pRham-NbSOS1 vectors. Cells were grown overnight at 37°C in LB medium supplemented with glucose 0.2% and kanamycin 50 μg/mL. On the next morning, cells were washed once in PBS prior to inoculation of culture flasks containing LB supplemented by 0.2% w/v L-Rhamnose to a final OD_{600} of 0.02. Cultures were grown to mid-exponential phase (OD_{600} 0.1) and treated with ofloxacin to a final concentration of 5 μg/mL, equivalent to 60-fold MIC (Goormaghtigh and Van Melderen, 2019). 10 μL samples were withdrawn at several time points after ofloxacin treatment (0 min, 30 min, 1, 3, 5h), diluted in PBS and injected into an Attune NxT flow cytometer (Invitrogen). 50,000 events were analyzed with a blue laser (488 nm) and a 530/30 emission filter. Subsequent analyses were performed using FlowJo 10.4 and MATLAB (R2017b, MathWorks) software, assisted by custom-made scripts.

Cell survival assay

Samples from *E. coli* SMR6669 test (transformed with pRham-NbSOS1) and control (transformed with pRham∅) cultures used in the previous experiment were collected at several time points (0 min, 30 min, 1, 2, 3, 4, 5h), opportunely diluted and plated on LB-agar to estimate the survival of bacteria to ofloxacin (CFU/mL). 5 independent replicates were measured at each time point, normalized by survival at time 0 and represented on a Log_{10} scale.

Filamentation assay

SOS-mediated arrest of bacterial cell division was evaluated by whole cell filamentation assay as already described by Bellio and coworkers, with slight modification to the original protocol (Bellio et al., 2020). Untransformed *E. coli* ATCC 25922 cells and cells of the same strain transformed with either pRham∅ or pRham-NbSOS1 vectors were grown overnight in LB liquid medium (supplemented by 50 μg/mL kanamycin in the case of plasmid-bearing cultures) at 37°C. The day after 10^6 CFU/mL of each overnight culture were inoculated into 10 mL of fresh LB or LB + Kan medium supplemented with L-Rhamnose 0.2% (w/v) and incubated for 1 h at 37°C under shaking. Ciprofloxacin at 1/8 of the MIC values (0.0078 μg/mL) was then added to the cultures to induce filamentation. Controls without ciprofloxacin were also included. Bacterial cultures were incubated for 3 h at 37°C in orbital shaker. Bacterial pellets were harvested by centrifugation at 18,000 g for 5 min at 4°C, washed twice with PBS, resuspended in paraformaldehyde (4% v/v in PBS) and kept in ice for 30 min. Samples were centrifuged and washed twice with PBS to remove paraformaldehyde residues. Aliquots of the resuspended pellets in 100μL PBS were spotted on polylysine coated glass slides and then left to air-dry overnight at room temperature. Slides were washed with distilled water before adding 80 μL of Fluoroshield with DAPI (4′,6-diamidino-2-phenylindole; Sigma-Aldrich) and then observed at fluorescent microscope (Zeiss AXIO Imager equipped with a Leica DFC350 FX digital camera).

MIC determination

Broth microdilution method was adapted to assess the susceptibility to ciprofloxacin of *E. coli* ATCC 25922 strains bearing either pRham-NbSOS1 or pRhamØ (empty vector, as reference) under the experimental conditions used throughout the RT-qPCR assays. A 96-well plate was prepared by pouring 270 and 100 μL of LB medium containing 30 μg/mL kanamycin and 0.2% w/v L-Rhamnose into each well of the first column and of the other 11 columns, respectively. 30 μL of the same medium supplemented by 1.5 μg/mL ciprofloxacin were added to column 1 and mixed by pipetting; then 200 μL of liquid medium were transferred to column 2. The same dilution process was repeated until column 11, from which 100 μL of medium were discarded. The last column was not subjected to ciprofloxacin supplementation (positive control). Single colonies of *E. coli* ATCC 25922 transformed with pRham-NbSOS1 (test culture) and empty pRhamØ (reference) were grown overnight in LB medium containing 30 μg/mL kanamycin, diluted to OD_{600} 0.5 in LB supplemented by 0.2% w/v L-Rhamnose and 30 μg/mL kanamycin and incubated 2 h at 37°C under shaking to induce NbSOS1 expression. A second dilution step to OD_{600} 0.1 was performed using the same medium as before, then 10 μL of diluted bacterial cultures were poured to each well of the previously assembled 96-well plate. Half of the plate was inoculated with the test culture and half with the reference culture. Each condition was assayed in triplicate. The plate was incubated statically at 37°C and OD_{595} was measured at 6 h using a plate reader (Tecan Infinite 200 PRO, Tecan Trading AG, Switzerland). Three wells containing only LB medium were used as blank and their average OD_{595} was subtracted to mean values of each triplicate. The ratio between samples subtracted mean OD_{595} and positive control values was calculated at each condition. These normalized data were represented versus ciprofloxacin Log-dose and fitted by a modified Gompertz equation (GraphPad Prism v.7.00), extrapolating the minimum inhibitory concentration (MIC) and 95% confidence intervals (CIs) values for both cultures.

QUANTIFICATION AND STATISTICAL ANALYSIS

The number of replicates performed for each experiment is reported in the corresponding method paragraph. Averages and errors (either standard deviation, SD, standard error of mean, SEM, or 95% confidence intervals) are reported in the tables, figures or captions, as well as details on number of replicates and statistical significance testing. Curve fitting was performed using GraphPad Prism v7.00, according to the models indicated in the respective method paragraphs.